PolyPublie
Polytechnique Montréal

POLYTECHNIQUE MONTRÉAL
UNIVERSITÉ D'INGÉNIERIE

Titre: Title:	Controllable Front-End Circuit for Geiger Mode Avalanche Photodiode
Auteur: Author:	Marzieh Ameri
Date:	2014
Type:	Mémoire ou thèse / Dissertation or Thesis
Référence: Citation:	Ameri, M. (2014). Controllable Front-End Circuit for Geiger Mode Avalanche Photodiode [Master's thesis, École Polytechnique de Montréal]. PolyPublie. https://publications.polymtl.ca/1349/

Document en libre accès dans PolyPublie
Open Access document in PolyPublie

URL de PolyPublie: PolyPublie URL:	https://publications.polymtl.ca/1349/
Directeurs de recherche: Advisors:	Mohamad Sawan
Programme: Program:	génie électrique

Ce fichier a été téléchargé à partir de PolyPublie, le dépôt institutionnel de Polytechnique Montréal
This file has been downloaded from PolyPublie, the institutional repository of Polytechnique Montréal

https://publications.polymtl.ca

UNIVERSITÉ DE MONTRÉAL

CONTROLLABLE FRONT-END CIRCUIT FOR GEIGER MODE AVALANCHE PHOTODIODE

MARZIEH AMERI

DÉPARTEMENT DE GÉNIE ÉLECTRIQUE

ÉCOLE POLYTECHNIQUE DE MONTRÉAL

MÉMOIRE PRÉSENTÉ EN VUE DE L'OBTENTION

DU DIPLÔME DE MAÎTRISE ÈS SCIENCES APPLIQUÉES

(GÉNIE ÉLECTRIQUE)

FÉVRIER 2014

© Marzieh Ameri, 2014.

UNIVERSITÉ DE MONTRÉAL

ÉCOLE POLYTECHNIQUE DE MONTRÉAL

Ce mémoire intitulé:

CONTROLLABLE FRONT-END CIRCUIT FOR GEIGER MODE AVALANCHE PHOTODIODE

présenté par : AMERI Marzieh

en vue de l'obtention du diplôme de : Maîtrise ès sciences appliquées

a été dûment accepté par le jury d'examen constitué de :

M. KASHYAP Raman, Ph.D., président

M. SAWAN Mohamad, Ph.D., membre et directeur de recherche

M. POULIOT Philippe, Ph.D., membre

DEDICATION

A happy family is but an earlier heaven

John Browning

To My Lovely Mom, Zohreh

To My Patient Dad, Mahmood

For making my earlier heaven more wonderful each day by being who they are

For their endless love, support and encouragement

ACKNOWLEDGEMENTS

One of the joys of completion is to look over the journey past and remember all the people who have helped and supported me along this long but fulfilling road.

I would like to express my sincere gratitude to Professor Mohamad Sawan for all his support, patience, generosity and advice during my master's studies in Polytechnique Montréal. His confidence in me gave me the power to overcome the difficulties and disturbances I had during this journey. It was both an honor and a privilege to work with him. He patiently provided the special vision and experiences in circuit design for biomedical applications.

I would not have completed this road if not for my parents, Zohreh and Mahmood, who instilled within me a love of creative pursuits, science and language, all of which finds a place in this thesis. Thank you both for giving me strength to reach for the stars and chase my dreams.

My great appreciation goes to my closest friend, Negin Javaheri, who was always a most reliable person and a great support in all the struggles and frustrations I faced. A special feeling of gratitude to my loving uncles, Masoud and Mohsen Ameri, whose words of encouragement and push for tenacity ring in my ears. And their support was always with me in this journey.

Also, I would like to thank all faculty members, staff, graduate students, and colleagues of Polystim lab who helped me during my education and research. Special thanks are due to the following people for their help and collaboration: Dr. Saeid Hashemi, Masood Karimian, Shahab Moazzeni, and Ahmed Hachani with whom I enjoyed the hours of friendly and stimulating technical discussions.

I would like to thank CMC Microsystems for providing access to design tools, technologies, and chip fabrication facilities.

RÉSUMÉ

L'objectif de recherche principal de ce mémoire est de concevoir et d'implémenter un circuit intégré visant à contrôler une photodiode à avalanche (Avalanche photodiode - APD) fonctionnant dans les deux modes : linéaire et Geiger. L'amélioration des performances liées à l'exécution de cette structure, comprenant la maximisation du taux de comptage des photons, la réduction de la consommation de puissance, ainsi que celle du bruit des circuits impliqués est parmi les principaux objectifs. Également, la surveillance en temps réel des caractéristiques d'une APD, en termes de tension de polarisation, de température, de rapport signal/bruit, de gain et du contrôle des effets thermiques, est considérée.

En raison de l'obtention d'un gain de courant trop faible dans le mode linéaire des APD, empêchant donc la détection de photons simples, le mode d'opération Geiger des APD a été choisi pour le système de comptage de photons conçu. De plus, puisque l'opération en mode Geiger exige un arrêt externe, le circuit *Quench-Reset* est utilisé pour détecter l'arrivée de photons, en détectant l'impulsion produite à l'arrivée d'un photon, et en réinitialisant l'APD afin de le préparer pour détecter le prochaine photon.

Un circuit rapide *Quench-Reset* a été conçu en technologie CMOS 0.18 µm, simulé puis fabriqué par la fonderie TSMC via les services de CMC Microsystems. Un assemblage (*wire-bounding)* spécial a été réalisé au laboratoire d'assemblage de Polytechnique (LASEM), affilié au laboratoire Polystim. L'interface du contrôle numérique du circuit intégré a été implémentée sur une plateforme FPGA hors puce. Un circuit imprimé (PCB) de test recevant le FPGA a été complété afin de tester et caractériser le circuit intégré fabriqué. Le circuit numérique est responsable du contrôle de l'effet de la température sur l'exécution de circuit APD en surveillant le gain dans les modes de fonctionnement linéaire et Geiger. L'effet thermique est contrôlé en changeant la tension de polarisation de circuit APD. Le code est développé dans Modelsim et mis en application dans un FPGA Igloo de la compagnie Actel.

Le moment d'extinction du circuit APD se situe entre 1 et 4 ns, tandis que le temps de réinitialisation est dans la gamme de 1 - 3 ns. La valeur la plus appropriée du temps *hold off* est unique pour chaque système et dépend de la nature, de la densité et de la durée de vie des maintient de photons associés à chaque APD; ainsi, le système est conçu de sorte à obtenir un temps *hold off* contrôlable dans la gamme de 4ns à 2µs. L'interface de contrôle du gain pour

rester indépendant des variations de la température est en mesure de faire le travail dans les modes linéaire et Geiger de circuit APD avec une variation de 10%.

Ce travail fait partie de la mise en oeuvre d'un système d'imagerie clinique non invasif et portatif entrepris par l'équipe de recherche multidisciplinaire Imaginc. Ce système communicant sans fil avec un ordinateur est basé sur l'acquisition de signaux NIRS/EEG (Spectroscopie proche-infrarouge/ électroencéphalographie), en temps réel, afin de produire une image du cortex entier tout en améliorant le confort du patient et prolongeant la période de balayage.

Ce projet est supporté par les instituts de recherche en santé du Canada (IRSC) et de la fondation des maladies du cœur.

ABSTRACT

The objective of this master's thesis is to design and implement a CMOS high-speed photon counting interface to be integrated within an Avalanche Photodiode (APD) operating in both linear and Geiger modes. Improving the main performance metrics of the structure including maximizing photon counting rate and minimizing both power consumption and system noise are among the objectives. Also, real-time monitoring of APD characteristics in terms of bias voltage, temperature, signal-to-noise ratio, gain, and extending control of thermal effects on APD performance are considered.

Since linear mode APD has low achievable current gain and therefore is not sensitive enough in detecting single photons, Geiger mode APD was selected for photon counting systems. Furthermore, since Geiger-mode operation requires an external stop, a Quench-Reset circuit was employed to detect photon arrival, count the pulse generated at photon arrival, and reset the APD in order to make it ready for the subsequent photon detection.

A high-speed quench-reset circuit was designed, implemented with 0.18 μm CMOS process, laid out and simulated and then fabricated by TSMC through CMC Microsystems. Wire bonding was done by LASEM facilities affiliated to Polystim laboratory. The control scheme of the whole system was implemented in an off-chip FPGA platform. For the sake of test and measurement, a PCB was made and test bench for digital part was implemented in FPGA. The scheme was responsible for controlling the effect of temperature on APD performance by monitoring the gain in both linear and Geiger modes of operation. The thermal effect was controlled through changing the bias voltage of APD. The code was tested in Modelsim and implemented to Igloo FPGA (Actel Co.). The chip was then tested using equipment available to Polystim and was characterized in terms of the performance metrics in question.

The quench time for the designed circuit was in the range (1 – 4)ns while the reset time was in the range (1 – 3)ns. The most appropriate value for hold-off time was unique for each system and it depended on the nature, density and lifetime of the traps of each specific APD; therefore the system was designed to have a controllable hold-off time in the range of 4ns - 2μs. The temperature-independent gain control system was capable of controlling the gain for both linear-mode and Geiger-mode APD in 10% variation.

This work is part of the multidisciplinary Imaginc research team to develop a clinical imaging system based on a real-time, noninvasive and portable NIRS/EEG (Near-infrared spectroscopy / Electroencephalography) signal acquisition system, which communicates wirelessly with a computer and images the whole brain cortex while improving comfort in long duration scanning. The presented work is part of a collaboration between Polystim research group , CIHR (Canadian Institutes of Health Research) and Heart and Stroke Foundation.

TABLE OF CONTENTS

DEDICATION iii

ACKNOWLEDGEMENTS iv

RÉSUMÉ v

ABSTRACT vii

TABLE OF CONTENTS ix

LIST OF TABLES xii

LIST OF FIGURES xiii

LIST OF SYMBOLS AND NOTATIONS xv

CHAPTER 1 INTRODUCTION 1

1.1 Project Overview 1

1.2 Basic Principles of Avalanche Photodiode 4

1.2.1 Multiplication Process 4

1.2.2 Operation Mode 7

1.2.3 APD Metrics and Features 9

1.2.3.1 Capacitance 9

1.2.3.2 Bandwidth 10

1.2.3.3 Quantum efficiency 12

1.2.3.4 Dark Count 12

1.2.3.5 After-pulsing 13

1.2.3.6 Leakage Current 14

1.2.3.7 Thermal Effect 14

1.3 Basic Principles of Quench-Reset Circuit 15

1.4 Research Objective and Challenges 17

CHAPTER 2 LITERATURE REVIEW 19

2.1 Quenching 21

2.1.1 Passive Quenching 22

2.1.2 Active Quenching 25

2.1.3 Further improvement 28

2.1.4 Thermal Effect Control 28

CHAPTER 3 QUENCH-RESET CIRCUIT: SIMULATION AND POST LAYOUT RESULT 31

3.1 Design Procedure 31

3.2 Simulation Result 37

3.2.1 Schematics 38

3.2.2 Post-Layout 41

3.3 Controller design for APD performance improvement 43

3.4 Chapter Conclusion 46

CHAPTER 4 EXPERIMENTAL RESULT: QUENCH-RESET CIRCUIT AND THERMAL EFFECT CONTROL 47

4.1 Quench-Reset IC 47

4.2 Control system 53

4.2.1 Controller 53

4.2.2 Temperature sensor 55

4.2.3 Test Bench 55

4.2.4 Control System Result 57

4.2.4.1 Linear Mode 57

4.2.4.2 Geiger Mode 58

4.2.5 Conclusion 59

CONCLUSION 61

REFERENCES 64

LIST OF TABLES

Table 4.1: Design characteristics 52

Table 4.2: I/O list of thermal effect control module for linear mode APD 57

Table 4.3: 1st Study case for thermal effect control module of linear mode APD – 2°C increase in ambient temperature 57

Table 4.4: 2nd Study case for thermal effect control module of linear mode APD – 2°C decrease in ambient temperature 58

Table 4.5: I/O list of thermal effect control module for Geiger mode APD 59

Table 4.6: Case study for thermal effect control module of Geiger mode APD 59

LIST OF FIGURES

Figure 1.1: Block diagram of a typical NIRS system developed for brain imaging 2

Figure 1.2: The APD gain in function of its reverse bias voltage 9

Figure 2.1: APD equivalent model 21

Figure 2.2: Passive Quenching: (a) Circuit, (b) Avalanche voltage and current behaviour 23

Figure 2.3: Active Quenching Circuit Concept 26

Figure 2.4: Active Quenching Circuit 27

Figure 3.1: Quench-Reset Overall: (a) system level block diagram, (b) expected signal 32

Figure 3.2: Circuit level design: (a) Quench Circuit, (b) Reset Circuit, (c) Digitizer, (d) Counter 33

Figure 3.3: (a) The quench circuit which consists of a level shifter and a quencher, (b) APD cathode voltage in absence of the quench circuit, (c) Level shifter Output, (d) Quencher Output 35

Figure 3.4: The functionality of digitizer block: (a) Input Signal, (b) Digitizer block, (c) Output Signal 36

Figure 3.5: The functionality of reset block : (a) Circuit design, (b) Detected signal by D-flip flop, (c) generated enable signal for Quench circuit 36

Figure 3.6: The feedback path of reset block 37

Figure 3.7: APD simulation model 37

Figure 3.8: Schematic simulation quench-reset circuit with no hold-off in term of APD voltage and output voltage: (a) 3 cycles of light impinging, (b) Zoom-in plot to indicate quenching time 39

Figure 3.9: Schematic simulation quench-reset circuit with 13 ns hold-off in term of APD voltage, output voltage and reset pulse: (a) 4 quenching cycle, (b) Zoom-in plot 40

Figure 3.10: Layout simulation quench-reset circuit in term of APD voltage, output voltage and reset pulse: (a) 3 cycles of light impinging, (b) Zoom-in plot 42

Figure 3.11: AC analysis of the Quench-Reset circuitry to estimate the bandwidth (BW) 43

Figure 3.12: Control algorithm to compensate the thermal effect : (a) Linear-mode Algorithm, (b) Geiger-mode Algorithm 45

Figure 4.1: The Layout scheme of the achieved Quench-Reset Circuit 47

Figure 4.2: The microphotograph of the whole fabricated chip 48

Figure 4.3: APD Model 49

Figure 4.4: Test setup of fabricated chip 50

Figure 4.5: Chip test result in response to: (a) one-shot light, (b) continues-wave light 51

Figure 4.6: Chip test result for reset circuit with: (a) hold-off time of 4ns, (b) hold-off time of 2µs 52

Figure 4.7: Igloo FPGA and FlashPro programmer 53

Figure 4.8: Different modules of the control unit built by a dedicated VHDL code 54

Figure 4.9: Control system test bench 56

LIST OF SYMBOLS AND NOTATIONS

ADC	Analog-to-digital converter SYMBOLS AND NOTATIONS
APD	Avalanche Photodiode
DAC	Digital-to-analog converter
FPGA	Field-programmable gate array
LED	light-emitting diode
MUX	Multiplexer
NIRS	Near-infrared spectroscopy
QC	Quench Circuit
RC	Reset Circuit
SNR	Signal to Noise Ratio
SiAPD	Silicon Avalanche Photodiode
TIA	Transimpedance Amplifier

CHAPTER 1 INTRODUCTION

1.1 Project Overview

The objective of this project is to design peripheral circuits for the avalanche photodiodes (APD) used as the detector of portable NIRS optical imaging technique. The signal detected by APD is the amount of attenuation of the re-emerging light from the near infrared light emitted through the scalp, skull dura and brain; therefore, an APD should be able to detect ultra-low amplitude light and thus it is important for an APD to have high gain. The designed circuits are responsible for quenching the bias voltage of APD operating in Geiger mode and controlling the gain for both linear-mode and Geiger-mode APD in 10% variation.

The key merits of portable NIRS optical imaging technique lie in the possibility of designing a non-invasive instrument that is unobtrusive, small size, low cost, low-power, and robust against motion artifacts.

A typical setup for a portable NIRS scanning device is shown in Figure 1.1 [1]. The setup often consists of a helmet bearing the light sources and detectors, the control module with built-in data acquisition circuit, and the interconnections. The main components of the helmet are light-emitting diodes (LEDs) as light sources and photodiodes as detectors. As the number of detectors increases, the spatial resolution in scanning images of the whole brain increases [1] [2].

Here, the interaction between light and tissue is a fairly complex issue at the microscopic level. Conceptually, the light source injects a given number of photons per unit time/volume/solid angle into a specific tissue spot where these photons travel inside the tissue along random trajectories [3]. Photons may pass several scattering events while traveling inside the tissues and a portion of them might be absorbed by the tissue. Eventually, only a fraction of photons may reach the detector and are captured by it.

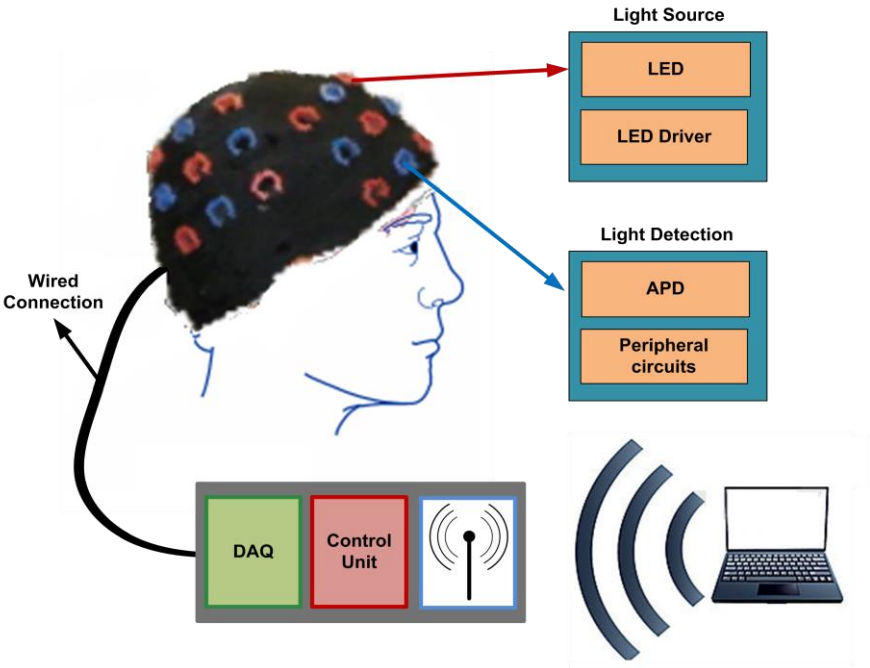

Figure 1.1 Block diagram of a typical NIRS system developed for brain imaging

On the other hand, to enhance the performance and accuracy of the NIRS system, highly sensitive photodetectors are required to convert the ultra-low amplitude light signal into detectable electric signal. There are only two options when it comes to choosing a photodiode that also amplifies the received light signal: a) photomultiplier (PMT) and, b) avalanche photodiode (APD). Unlike the PMT, APD works quite well for near-infrared light level with comparatively lower bias voltage and lower power consumption and it is relatively insensitive to magnetic fields. The latter results in having less noisy signals in magnetic areas, which makes it much easier to combine with other brain imaging devices such as MRIs. Therefore APD can be a proper candidate for the applications with high-magnetic-field. Moreover, APDs are also recognized for their simple and monolithic structure, compact, lightweight, mechanical robustness and long life [4]. Thus APDs are generally useful in applications where space is at a premium or where the detector may be subjected to shock or vibration.

Having high quantum efficiency (80%) in near infrared is another advantage of APDs in comparison to PMTs. Quantum efficiency is the efficiency with which light is detected. In a typical PMT, only 10%-30% of incident photons are converted into photoelectrons at the photocathode, and even this efficiency is achieved only over a narrow spectral range. In contrast,

in addition to superior quantum efficiency (as high as 80% at 900 nm), APDs offer a wider spectral range of 250 nm to 900 nm. Therefore, the photodetectors implemented for portable NIRS are APDs.

NIRS portable systems could be evaluated by different parameters; among them, size, portability and cost are of significant value. It is of great interest to integrate APD along with a peripheral circuit with advanced sub-micron CMOS process. This way, choosing appropriate substance/structure and adequate process for the design of an APD and the peripheral circuits becomes of great concern. For APD structure to operate in near infrared range, materials such as silicon (Si), InGaAs and Germanium (Ge) are suggested, among which silicon is preferred due to its excellent crystal quality, low excess noise, low cost, low temperature dependence [22], high gain and large bandwidth. Silicon APDs are also known for great performance in Geiger mode of operation with dark counts in the range of a few counts per second [5]. Another characteristic that makes silicon the most promising candidate for APDs is its low ionization coefficient ratio ($k < 0.1$) [5] [6].

Silicon APDs incorporate an absorption layer for incoming photons to produce electron-hole pairs in this region, as with any other photodiode. However, APDs operate with a large reverse bia voltages. The high internal field accelerates the photon-generated electrons. These electrons collide with the atomic lattice, in a recursive manner leading to an avalanche-like process. Avalanche multiplication relies upon extremely high internal electric fields on the order of 10^5 V/cm to drive the ionizing collisions of carriers with the lattice. The small bandgap of materials sensitive to long-wavelength light means that such high fields can cause tunneling between bands: an unwanted source of dark current. The multiplication layer is designed to provide the desired gain while suppressing noise. The performance of silicon APDs in infrared range could be improved by replacing this layer with a low-bandgap and highly-absorbing material such as InGaAs or Ge to absorb long-wavelength light in a single dedicated absorption layer, while the multiplication layer remains silicon. Doping is used in an adjacent charge layer to keep the potential low across the absorption material, so that only the multiplication layer experiences extreme fields. For this purpose, Ge is preferred as it is possible to develop APDs with CMOS-compatible process [6]. Adding Ge or InGaAs however complicates the process and increases the cost significantly. In this project, silicon APD is chosen due to requiring low operating voltage, exhibiting high quantum efficiency, and bearing low cost for near infrared

range applications. Taking the advantages of implementing an APD, fabricated with CMOS-compatible processes along with CMOS-integrated circuit technologies may result in realizing on-chip high-performance NIRS systems. Such implementation also serves our objective of fabricating portable, ultra-high sensitive and low-power NIRS systems and peripherals while saving used silicon area.

1.2 Basic Principles of Avalanche Photodiode

1.2.1 Multiplication Process

In an APD, when exposed to a light source, the light is absorbed in the depletion layer of the reverse biased p-n junction, and electron-hole pairs are generated. This is due to the light energy being greater than the bandgap energy in typical applications. Recall that the bandgap energy depends on material properties and is greater than 1.1eV for silicon. The internal electric field across the depletion region, when biased in reverse direction, drives the electrons towards the n+ side while it drifts the holes towards the p+ side. As the reverse bias voltage increases, so does the electric field, which leads the carriers (mostly electrons) to accelerate. The carriers then gain sufficient energy from the electric field and collide with the crystal lattice. This collision leads to generation of another electron-hole pair while losing some of carriers' kinetic energy. The process is called impact ionization [7] and is defined as the ability to create a secondary electron-hole pair for a carrier by gaining enough energy, and depends only on the local electric field [8]. The multiplication mechanism can be analyzed with reference to ionization rate and it is defined as the number of electron-hole pairs generated during the time that a carrier moves a unit distance. The ionization rates are denoted as α and β for electrons and holes, respectively. For silicon, the ionization rate of electrons is larger than that of holes ($\alpha > \beta$), so the electrons contribute more to the multiplication. The rate of ionization is reversely proportional to temperature; that is, as the temperature decreases, energy loss for photon scattering decreases and the ionization rate increases [9]. As a result of impact ionization for both electrons and holes, additional carriers are generated. By traveling through the high electric field, the newly generated carries obtain enough energy to trigger additional impact ionizations. This leads to a phenomenon called *avalanche*. After a few transit times, a competition develops between the rate at which

electron-hole pairs are being generated by impact ionization and the rate at which they exit the high-field region and are collected. If the magnitude of the reverse-bias voltage is below the breakdown voltage, collection wins the competition, causing the population of electrons and holes to decline. Each absorbed photon creates on average a number of electron-hole pairs (*M*), where *M* typically lies in the range from tens to hundreds [10]. The internal gain, *M*, also called multiplication gain, differentiates APDs from other photodiodes, and represents the amplification of the generated carriers. Multiplication gain for an APD with uniform electric field and ionization rate across the multiplication region with *W* width can be calculated through equation (1-1) [11]

$$M = \frac{1-k}{exp(-\alpha W[1-k]) - k} \tag{1-1}$$

where $k = \frac{\beta}{\alpha}$ is called ionization rate ratio.

The above equation is used when electrons are injected into the avalanche region. The same expression can also be used for holes by replacing k with $1/_k$.

For most of silicon APDs, the electrons are injected into the avalanche region, which means $\beta < \alpha$, therefore $k < 1$ [5].

As the bias voltage increases, the multiplication drastically increases until the device reaches a point at which it experiences a large short circuit current and hence cannot be used as a detector. The voltage at which the multiplication gain would be infinite is called breakdown voltage, which is when the denominator of the equation (1-1) becomes zero. It is evident that the breakdown voltage for a device with thicker multiplication region is larger than its thinner counterpart. The ionization profile for each carrier is not uniform as they experience different conditions. Therefore during the multiplication process, the device is subject to an incremental noise. Such excess noise could be described as follow:

$$N_{excess} = M(2qFI)^{1/2} \tag{1-2}$$

where q is the charge of an electron and I is the sum of the photo-current generated at M=1 and the dark current multiplied component. M is the multiplication gain and F refers to excess noise factor, which can be expressed as follows: [12]

$$F = Mk + \left(2 - \frac{1}{M}\right)(1 - k) \tag{1-3}$$

where k is the ratio of the hole/electron impact ionization rates. Here, similar to gain equation, it is assumed that the electrons are solely injected into the avalanche region. Equation (1-2) could be extended to evaluate the gain for the injected holes, once k is substituted by $1/k$.

For the ideal minimized noise, k is considered to be zero and infinity for electron and hole injections, respectively.

Statistical noise, defined as equation (1-4), should further be considered which incorporates the transformation mechanism from photons to electrons. It indicates that the ionization rate is not deterministic and has statistical fluctuations.

$$N_{Statical} = (2qI_{ds})^{1/2} \tag{1-4}$$

where q is the charge of an electron and I_{ds} is the dark current for non-multiplied component.

Considering equations (1-2) and (1-4), the shot noise of an APD (I_n), consisting of excess and statistical components (I_n), could be formulated as follows:

$$I_n^2 = 2q\left(I_L + I_{dg}\right)BM^2F + 2qI_{ds}B \tag{1-5}$$

where B is the noise bandwidth, F is excess noise factor, M is multiplication gain, I_L is photocurrent at M = 1, I_{dg} is dark current multiplied component, and I_{ds} is the dark current non-multiplied component.

The APD is also subject to thermal (dark current) noise due to load resistor which is given by eq. (1-6)

$$N_{termal} = \frac{4k\,T\,B}{R_L} \tag{1-6}$$

where k is Boltzmann's constant, T is absolute temperature, and R_L is load resistance.

The APD total noise current is the sum of thermal and shot noises. Note that the total RMS noise of a system is equal to the square root of the sum of all the noise components. It is shown in [29] that for a detector where the only source of noise is dark current, the signal to noise ratio (SNR)

for a fluorescence signal of 10^7 photons/sec would be ${}^{10^7}/_{10^3} = 10^4$. Here, the author assumes that the dark current rate (DCR) of the detector is 10^6 counts/second and it follows Poissonian distribution.

To maximize SNR, for a given input signal power, the noise should be minimized. In case of an ideal APD, where the dark (thermal) noise is zero, the only source of noise is statistical noise. This class of noise, as already stated, is related to transformation from photons to electrons. The ideal SNR is given by:

$$SNR = \frac{{I_L}^2 M^2}{2q\ B\ I_{ds}} \tag{1-7}$$

The common source of light may not be capable of providing sufficient luminance. Consequently, it is often needed to amplify the signal while holding the noise profile at low level. There are two solutions which can be presented for such a problem: a) adding preamplifier and amplifier stages and b) making use of detectors with intrinsic gain. The former solution, however, may lead to an increase in the required area and complexity. It is worth noting that although an APD introduces excess noise due to multiplication process, the amount of noise is still lower in comparison to the noise generated from connecting an external amplifier to a conventional photodiode operating at high frequencies.

1.2.2 Operation Mode

An APD can generally work in either linear or Geiger mode. The mode of operation depends on the magnitude of the reverse bias voltage across the p-n junction with respect to the breakdown voltage.

In order to operate in linear mode, the reverse bias voltage is kept below the breakdown voltage of the junction and the photo-generated charges are amplified with a finite multiplication gain. In this mode, the average photocurrent is shown to be proportional to the incident optical flux, and the multiplication gain hence can be calculated as follows [13]:

$$M = \frac{1}{1 - [\frac{V_b}{V_{Br}}]^m} \tag{1-8}$$

where *m* is a constant value for a particular APD; which depends on the substrate material and its value ranges between 2 and 6. V_b and V_{Br} represent the reverse bias voltage and the breakdown voltage, respectively, while *M* stands for multiplication gain.

In this mode of operation for an APD, the avalanche multiplication process induces a measurable current by amplifying the negligible current generated by photons. Despite amplification, such multiplication gain is still low due to existing statistical fluctuations in the multiplication process [3]. Therefore, an APD operating in linear-mode does not have enough sensitivity to detect single photons.

On the other hand, enforcing an APD to operate in Geiger-mode requires the reverse bias voltage to be higher than the breakdown voltage. This ensures that the primary signal gain is sufficient to count single photon. In this mode of operation, APD works as a triggering rather than an amplifying device. In fact, an APD operating in Geiger mode gives rise to a detectable macroscopic current due to high electric field and the run-away avalanche phenomenon induced by the creation of a single carrier. However, a macroscopic current would swiftly build [14] and self-sustaining avalanche process would continue, thus rendering the device useless for subsequent detections until it stops externally. The process may also stress the device and lead to a damage which affects its performance and crosses the liability boundaries. Therefore, operating in this mode requires applying an external stop which is essential to lead APD in a new detection sequence [15]. Moreover, in the Geiger mode, the internal amplification of APD, which is the result of the avalanche multiplication process, provides virtually infinite gain to the photo-generated current. Such infinite gain further results in all the current pulses to have the same amplitude. As a result, for an APD operating in Geiger mode, the amplitude of signal does not bear significant information [4]. In this case, counting the number of pulses occurring as a result of photon detection is of great interest. The photon counting rate is estimated either by counting the number of events in a time interval with a certain duration or by measuring the time gap between two consequently detected pulses.

The gain resulted from receiving a single photon in Geiger mode APD can be calculated as follows [16] :

$$G = \frac{V_{ex}C}{q} \tag{1-9}$$

where C is junction capacitor, q is electron charge and V_{ex} is excess voltage given by $V_{ex} = V_{Bias} - V_{Br}$.

For an APD biased in reverse polarity, the reverse current increases very rapidly at high bias voltages due to avalanche phenomenon. As indicated in Figure 1.2, for a typical photodiode prior to triggering avalanche process, the gain is equal to 1. Yet, for an avalanche photodiode operating in linear mode, the gain value ranges from 10 to 200. This gain is found to vary between 10^4 and 10^9 for an avalanche photodiode operating in Geiger mode.

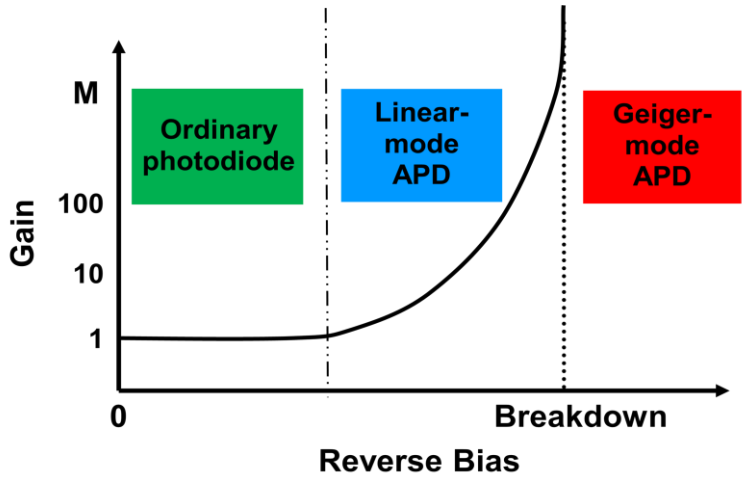

Figure 1.2: The APD gain in function of its reverse bias voltage

1.2.3 APD Metrics and Features

There are several parameters associated with an APD in different modes of operation. Here we address the major parameters as following:

1.2.3.1 Capacitance

An APD, like any other photodiode, exhibits different capacitances based on the polarity of the supply voltage. In forward bias, the capacitance associated to APD is related to charge-storage in semiconductor interface. This is not the case for a reversely biased APD where the capacitance is mainly due to the depletion region formed between semiconductors of different types. Therefore,

the former is not applicable for Geiger-mode APD [17]. Since the junction capacitance depends on the depletion layer thickness, it could be employed as a measure to find out the depth of the depletion layer. If carriers are generated outside the depletion layer, they cause problems such as slow signal decay time. Therefore, to ensure high-speed response, it is necessary to apply a reverse voltage which makes the depletion layer thicker than the penetration depth of the light into the light absorption layer [18]. For the APD with an active area of A and a depletion area width of W, the junction capacitor is expressed as follows:

$$C_j = \frac{\epsilon A}{W(V_{bias})} \tag{1-10}$$

where ϵ is the permittivity of dielectric.

From Eq. (1-10), C_j increases with increasing APD active area and/or decreasing depletion thickness. On the other hand, the transit time of charge carriers in an APD increases with an increase in the thickness of APD depletion layer. Therefore, choosing the APD thickness would imply a performance trade-off between noise and speed [19] [20]. Eq. (1-10) corroborates that the capacitance has an inverse relation to bias voltage; therefore, by increasing bias voltage, APD capacitance would decrease.

1.2.3.2 Bandwidth

The bandwidth of an APD photodiode is primarily determined by; a) electron and hole transit times, b) R-C time constant, c) minority carrier diffusion length, d) the number of carrier trappings, and e) signal delay due to photodiode packaging [21].

The transit times depend on the thickness of the active area and the electron/hole saturation velocities. Thus, the thinner the absorbing layers are, the shorter the transit times will be.

The RC time constant is determined by the APD equivalent circuit parameters. Junction capacitance, which is defined as the edge of the depletion region (or space charge region), and parasitic capacitance, which depends on the metallization geometry, can be considered as the APD capacitance. The APD resistance consists of series resistance, which is caused by the Ohmic contacts, and bulk resistances, and load resistance. By considering R_S and R_L as the series and load resistors, and C_J and C_P as junction and parasitic capacitors, the electrical 3-dB bandwidth can be approximated as follow [22]:

$$f_{3dB} = \frac{1}{2\pi(C_J + C_P)(R_S + R_L)} \quad (1\text{-}11)$$

Diffusion current is important for APDs since significant absorption occurs in depletion region, which is outside of the high-field region. Those carriers within about one diffusion length of the depletion region will have a chance to diffuse into the active region. The diffusion current will contribute a slow tail to the detector impulse response and may be reduced to some extent by recombination in these highly doped contact layers [22] and would deplete the entire absorbing layer [21].

In some APD designs such as hetero-structures, the bandwidth may be limited by the occurrence of carrier trapping of electrons at conduction band discontinuities and trapping of holes at valence band discontinuities [22]. Hole trapping is a significant problem in long-wavelength photodetectors due to the large valence band discontinuity at the InP / InGaAs heterojunction [22]. Researchers have reported solutions such as applying a moderately high electric field across the hetero-interface. Another technique suggests grading the band discontinuity with a compositional alloy [21].

Packaging and any external connections to the photodetector often limit the detector performance. Having a high impedance load and a reflection coefficient close to unity are other problems of photodiodes. A solution to this problem is to integrate a matching resistor with the device and using a lower contact layer without adding any additional mask or process steps [22]. The disadvantage of a load resistor is the reduction in effective quantum efficiency since some of the photocurrent goes through the matching resistor [22].

Another influential parameter on APD bandwidth is terminal capacitance. In fact, APD capacitance along with its input series resistance, form a circuit the time constant of which is affected by capacitance. This time constant should be respected throughout the normal operation of APD, which involves consequent charging/discharging of the detector. APDs with larger capacitances, when compared to their counterparts, are subject to narrower bandwidth. Decreasing the photodiode active area lowers junction capacitance and as a result reduces the *RC* time constant. However, a small device area can result in high contact resistance, which will increase *RC* constant. Packaging-induced parasitic effect may also cause bandwidth degradation. The issue may be overcome by making use of advanced bonding techniques [21]. The external

bias circuit is a difficulty in very high speed devices is the difficulty in building external bias circuits. The necessary bias capacitor and load resistor can be integrated with APD without adding any additional mask or process steps by using a large area region as the capacitor and the lower contact layer as the series resistor [22].

1.2.3.3 Quantum efficiency

There is a possibility for an absorbed photon in the active region of an APD to generate a primary carrier, and to eventually trigger an avalanche process. Such possibility is called quantum efficiency (QE). The ideal value for QE is unity, i.e., all the photons are absorbed in the active region. As the wavelength becomes larger, the chance of the photon being absorbed through the active portion of the depletion layer decreases. For short wavelengths (<400nm), the photon generated in the surface may be immediately absorbed. Quantum efficiency mainly depends on APD structure and antireflection (AR) coating on the diode window. Typical values of QE for APD range from 40% to 80% [23].

1.2.3.4 Dark Count

Dark count rate (DCR) is defined as the number of avalanches triggered while there is no light impinging on the active area of the APD. Dark counts are highly dependent on the doping of the junction and the characteristics of the fabrication technology. Modifying the doping profile of implants may mitigate the effect. APD active area also affects DCR in a non-linear fashion [24]. DCR can generally be used to characterize dark current, which is considered as a major source of intrinsic noise in APDs. There are two major sources for dark current; a) random thermally-generated electron-hole pair, and b) tunneling [25].

The minority carriers inside an APD may gain enough thermal energy from the substrate to diffuse into depletion region. On the other hand, for Geiger-mode APD, the device experiences large electric fields across depletion region due to reverse biasing; which may cause some of the minority carriers to drift into the depletion region and accelerate across it [13]. The thermally-generated electrons also have multiplication effect. At lower temperatures, the carriers have less energy and thus their random motion decreases.

On the other hand, tunneling is mostly a design-based issue and is affected by the properties of the materials of choice. Recall that for a design where APD is subject to small negative bias

voltage, the width of the depletion layer is very thin. Moreover, for an APD implemented using semiconductor with small bandgap property, the carrier quasi-Fermi level (i.e. the displacement of the population of holes and electrons from equilibrium) can overlap. For both conditions, the carrier tunneling across the depletion region may by triggered and thus the tunneling current occurs under reverse bias [26].Tunneling can be controlled by compromising vital properties like bias voltage [27].

It is of great interest to hold the dark count noise as low as possible. The objective could be served by enforcing APD to operate at temperatures and excess voltages as low as possible. For a typical APD, DCR ranges from 1 to 10^6 counts/sec. If the DCR exceeds this range, for example higher than 10^7, APD operates in saturation region and the signal will be inundated with dark noise [28].

1.2.3.5 After-pulsing

During an avalanche, some of the carriers, crossing the depletion region, are captured at deep levels inside the junction and are stored in traps in the APD. These carriers can release after a random period of time. As the stored charges release during the active period of APD, an avalanche current occurs. The resulting current is due to a previous avalanche event, but not related to a new photon arrival. The new avalanche event, in turn can lead to further carrier trapping, and this cycle continues. This unwanted source of noise is called after-pulsing.

After-pulsing intensity depends on: a) the number of carriers crossing the junction, b) trap density and c) temperature. The number of carriers crossing the junction is directly related to the total charge of the avalanche event, while the total charge and current intensity depends on the over-voltage. In addition to trap density, how deep inside the junctions the released carriers were trapped indicate the release period of each of the carriers, and therefore the onset of after-pulsing [29]. The density of deep-level traps can be reduced by improving material quality which can be a method for decreasing after-pulsing. However, material improvement is usually a relatively difficult task [28]. Another effective parameter on after-pulsing is temperature: as temperature increases, the trapped carriers escape more rapidly and thus the after-pulsing effect is less. Although an increase in temperature decreases the after-pulsing effect, at the same time it leads to increased thermal generation, causing higher dark count rate. The choice of the optimum

temperature is important in order to keep after-pulsing effect and dark count rate at the least possible value.

After-pulsing is the major limitation on operation of APD as photon counter at high repetition rate [29] and it limits the high frequency operation of APD. By keeping the voltage across the APD below the breakdown voltage after each photon detection for sufficiently long time, trapping centers can be empty and the after-pulses may not be generated anymore. The sufficient time should be longer than the trap emission lifetime. However, when speed is important and the repetition rate gets closer to the trap emission life time, after-pulsing effect increases.

1.2.3.6 Leakage Current

The leakage current is generated as a result of the voltage across the photodiode in the reverse bias, and it is directly related to the size of the photodiode. With smaller photodiodes, the leakage current will be lower. The total leakage current is the sum of the surface leakage current and the volume leakage current:

$$I_{L-Total} = I_{L-Surface} + I_{L-Volume} \quad (1\text{-}12)$$

The surface leakage current is the amount of leakage current between the p-doped and the n-doped regions in contact with the SiO_2 passivation layer. These leaks are related to the circumference of the photodiode. The volume leakage current is the amount of leakage current between the p-doped and the n-doped regions, in the volume of the junction (plane, cylindrical and spherical). These leaks are related to the area of the photodiode (diffusion depth, length and width of the junction).

1.2.3.7 Thermal Effect

As a result of impact ionization in the high electric field region of APD, electron-hole pairs are generated which result in avalanche multiplication. Although carriers gain energy from the applied electric field, some of this energy will be transferred to lattice vibration. This energy loss is caused by various scattering mechanisms, of which phonon scattering will ultimately dominate due to strong interaction between carriers and the lattice vibration [21]. The free mean path length of carriers has an inverse relation with temperature [21], and it would decrease by an

increase in temperature. This means that carriers are scattered more frequently at elevated temperatures.

On the other hand, as mentioned in sections 1.2.3.4 and 1.2.3.5, both DCR and after-pulsing processes are temperature dependent. If the temperature is not low enough, the dark counts would be high. The high dark counts occur when thermal generation triggers avalanche events, and cooling the APD is a solution to this impact. In contrast, if the temperature is not high enough, the after-pulsing effect would increase. As noted in 1.2.3.5, there is always the possibility that the carriers become trapped inside the crystal and get released later. By reducing the temperature, the lifetime of trapping events increases, which results in an increase in after-pulsing. Therefore there is a trade-off between minimizing dark counts and after-pulsing by controlling the temperature.

Another APD parameter strongly affected by junction temperature is breakdown voltage (V_{br}). The thermal coefficient of breakdown voltage depends on the APD device structure and is usually fairly high, typically around 0.3%/K [28]. At constant bias voltage supply, an increase in breakdown voltage V_{br} causes a decrease in over-voltage V_{ex}, and therefore it results in reduced photon detection efficiency and causes non-linear distortion in photon counting.

1.3 Basic Principles of Quench-Reset Circuit

Due to disadvantages of APDs which are long transit times and excess noise, associated with the stochastic APD multiplication process, several high-speed CMOS front-end circuits have been proposed in the past few years to overcome these limitations [19] [30]. As mentioned in section 1.2.2, in the linear mode, there is a limitation on the maximum achievable gain. Therefore in this mode, APD has to be followed by a transimpedance amplifier (TIA) front-end. TIA converts the output current to voltage with maximum SNR for following stages of the receiver for further processing [31]. However, operating in linear mode for APD means having the low achievable current gain, and therefore not being sensitive enough to detect single photons. To detect single photons, APDs must be operated in Geiger mode. Furthermore, since Geiger-mode operation requires an external stop, the Quench-Reset circuit is employed to detect photon arrival, count the pulse generated at photon arrival, and reset the APD in order to make it ready for the next photon detection. The idea is to keep APD in an extremely sensitive condition (i.e., few

volts above the breakdown voltage) in a way that by absorbing a photon and triggering an avalanche, a huge increase in output current occurs. At this point Quench-Reset circuit should be active to quench (shut-off) the avalanche and return APD to the sensitive state. When the avalanche is quenched the current becomes zero, and the voltage slowly returns to its previous value.

In each quench-reset circuit, quench time is defined as the time elapsed from the onset of the avalanche until it is quenched; which means the time it takes to interrupt the avalanche multiplication process and shut off the avalanche current by increasing the APD's bias voltage above breakdown. In the same circuit, reset time is defined as the time required for bringing back the APD to its original quiescent state.

If the reset action happens immediately after quench process, the chance of having after-pulsing increases. One solution to reduce the amount of after-pulsing, besides fast quenching [19] (which means reducing the avalanche charge and current intensity rapidly), is to wait for all the trapped charges to dissipate without triggering additional avalanches before resetting process. This can be achieved by keeping the APD in the OFF state for a period of time in between the quench and reset process. The mentioned period is called Hold-off time. The period of hold-off time depends on the nature, density and lifetime of the traps of each specific APD. It should be long enough to allow trapped carriers to be emitted and not to allow the after-pulsing affect the photon counting statistics. Studies show that if the hold-off time is less than the mean trap lifetime then after-pulsing will significantly affect the photon counting statistics [32]. Meanwhile, Hold-off time should not be too long to avoid limiting the repetition rate and affecting the validity of the counting statistics. Therefore most appropriate hold-off differs from one APD to another, and having controllable hold-off time circuit is highlighted. The sum of quench time, hold-off time and reset time is called dead-time, which can be defined as the minimum delay that must elapse between two consecutive avalanches in order for both to be detected.

Another important portion of dead-time is reset time. Reset time should be as short as possible: with long reset time, the chance of the avalanche triggering during reset time increases. On the other hand, the effective bias voltage varies with time. This variation can cause some pulses to be missed from photon counting; since, the output pulse from the early avalanche triggering may be

too small to be detected and the counting rate would be affected. Long reset time can also affect APD's performance, such as detection efficiency and timing response.

Having the peripheral circuits (TIA and Quench-Reset circuit) integrated with APD on the same chip, adds some advantage to the system such as reducing after-pulsing, increasing sensitivity, and lowering power consumption. CMOS 0.18 µm technology is the chosen process for fabrication.

The ability of APD avalanche multiplication in amplifying the photon-generated signal makes it well-suited for detecting extremely weak light intensities, such as the one associated with low-amplitude reflected NIR signal. However, it is not always simple to gain the desired magnitude for the amplified signal. It is due to the need for a high reverse voltage and a large multiplication gain which is, among other facts, temperature dependant [5]. Therefore, employing a control unit is essential to eliminate the effect of temperature and to improve the performance of APD, accordingly.

1.4 Research Objective and Challenges

This Master's thesis investigates the design and implementation of an integrated building block intended to tune an APD with improving its performance in term of maximizing the photon counting rate and minimizing power consumption and system noise. This system should be capable of real-time monitoring of the APD's gain and keeping its variation in a pre-defined range.

The quench-reset circuit should be a circuit with high photon counting rate, low power consumption and small size. Having controllable hold-off time is another objective of this circuit. The circuit should be designed to be integrated on the same chip as the APD to reduce after-pulsing, increase sensitivity and lower power consumption. To allow connection to other designed components of the project, the quench-reset circuit should be fabricated in CMOS 0.18 µm technology.

To improve the performance of the APD, some of its parameters need to be monitored in real-time, and corresponding values would be calculated based on the monitored parameters. This goal is achieved by an off-chip control system. Bias voltage, temperature, and gain are the

mentioned parameters and features. As a result, a temperature-independent gain control loop is designed by controlling and changing the bias voltage for linear and Geiger mode APD. The aim is to choose the best controller device in terms of small size, user-friendly monitoring, and compatibility to different sensors to be able to analyze as many parameters as possible.

Thesis Organization

Chapter 1 presented an introduction to the IMAGINC portable NIRS brain imaging device. The avalanche photodiode and its limitations to work in linear and Geiger modes were reviewed. Several of its physical parameters were outlined, and the effect of temperature on some of the parameters was studied. The quench-reset circuit was introduced, and the related concepts were reviewed.

Chapter 2 presents a literature review on different CMOS quench-reset (QR) circuits, including advantages and disadvantages of each passive, active, and mixed circuits. Different systems used to control the thermal effect on the performance of APDs are also reviewed.

In *Chapter 3,* designing quench-reset circuits are discussed, providing explanation on their functionality and simulation results. A control system is designed to monitor APD parameters and performance, and a temperature-independent gain control loop is designed based on changing the bias voltage.

Chapter 4 covers experimental results of the fabricated quench-reset circuit integrated in a CMOS chip. The overall platform is also discussed in this chapter. The unit consists of the control system to improve the APD performance in both linear and Geiger modes, the quench-reset circuit dedicated for the Geiger mode APD and a TIA circuit when APD performs in linear mode.

Chapter 5 is presented as a summary of the project along with comments concerning recommendations for future work to design fully integrated CMOS device including the APD, its quench-reset circuit, as well as control circuit of various parameters on the same chip.

CHAPTER 2 LITERATURE REVIEW

Finding a technique for photon counting is necessary when the amount of light is extremely low; in this case, conventional analog measurement of light intensity becomes extremely difficult. In the 2000s, the concept of a new generation of photon counters introduced which was called SiPM (Silicon-Photomultiplier). In January 2008 it was commercialized under the name of Multi-Pixel Photon Counter (MPPC) by Hamamastsu and as SPM (Silicon Photomultiplier) by SensL. SiPM is the matrix of photodiodes (e.g. 32x32 = 1024 photodiodes) polarized in Geiger mode, forming a single undividable detector surface area of a few millimeters [16] [33]. Each photon generates a current pulse, and at the detector output, counting the number of pulses represents the number of photons received. In order to have an accurate measure of counted pulses, it is important to have the width of the pulses as short as possible to avoid missing any photon; meanwhile the invalid pulses should be filtered.

For many applications where very low-levels of light are to be detected, it is desirable to use a detector with high sensitivity; namely, a device with high optical gain. The Avalanche Photodiode has been developed for this purpose, which is essentially, as anticipated, a PIN diode with high gain.

The idea of avalanche photodiodes was introduced in the 1950s, and became a popular research area in the 1960s and early 1970s, with both linear-mode and Geiger-mode functions being topics of interest. Limited electric fields and high fabrication cost of photo-multiplier tubes (PMTs) were two main motivations to introduce APDs as both a signal amplifier for low-flux imaging applications and as a means to detect single photons [34]. As research fueled development, other advantages of APDs were revealed; offering digital-mode operation for single-photon counting [34], high gain and high sensitivity. In the 1960s, Haitz's group introduced the avalanche phenomenon in p-n junctions biased above the breakdown voltage; a model of this device was presented [35]. An APD is basically an advanced PIN photodiode but with faster timing. By way of comparison to other PIN photodiode, APDs are associated with internal gain, which means

more than one signal carrier is generated per photon. Without gain, the electrical signal due to photon flux is usually lost in readout noise.

In the 1970s, during the early development of silicon APDs, the statistical properties of the avalanche phenomenon were provided by McIntyre and Webb [36] [37]; the single-photon generated pulses were observed in their APDs biased above breakdown voltage [38]. Advances in electronics have reduced the inherent noise and the breakdown voltage of APDs, which makes them a suitable option for portable devices.

Sensitivity and signal-to-noise ratio can be enhanced by reducing the noise. The major source of noise is dark noise which depends on both junction temperature and the reverse bias voltage. Rather than cooling the device, operating APD under low biasing condition is important [39].

Another method to increase sensitivity is to enhance the gain. Although APD has the advantage of high gain in comparison to PIN photodiodes, the gain in linear mode is not as high as PMTs. Internal gain for APD operating in linear mode is 200-1000 while PMT typically has an internal gain of $1x10^5$ to $1x10^7$ [40]. To boost the APD gain, external amplification is required, and a transimpedance amplifier is the solution to produce similar intensity signals between an APD and PMT [40]. However, increasing the gain in this mode increases noise because the noise would be also multiplied by the gain. Therefore, APD operated in Geiger mode is studied where bias voltage is greater than breakdown voltage [41].

The optical gain is defined as the number of carriers generated as a result of the absorption of a single photon. The optical gain for Geiger-mode APD is virtually infinite. The Geiger mode is also called single-photon detection mode; since instead of a linear gain relation between the generated photocurrent and the number of incident photons, it gives a digital pulse per avalanche event [41]. The light intensity can be obtained from photon flux, which can be attained from counting the photon events over a period of time. The sensitivity of Geiger-mode APD is limited by dark count noise, which counts the events as the result of thermal generation of electron-hole pair instead of incident photons [41]. As explained in previous chapter, as the result of avalanche multiplication in Geiger-mode APD, a macroscopic current is triggered, and a sharp pulse is produced which can be counted. The leading edge of the generated pulse marks the photon arrival time very precisely. The self-sustaining current continues flowing until the electronic field is reduced below breakdown onset. The final steady state current will be governed by the series resistor (R_S) of the circuit [42]. Meanwhile, the device will have no response to any other

incident photon. To externally stop the self-sustaining current and perform high-speed photon counting, an APD is used in conjunction with a quench circuit, which can be passive, active or gated. This is achieved by lowering the bias voltage below the breakdown voltage, which is done by quenching procedure.

2.1 Quenching

Different solutions and circuits have been proposed for the quenching process; however, all different types of quenching circuits have two main common purposes: to quench the avalanche current by lowering the voltage below breakdown after triggering an avalanche current, and to reset the device for subsequent detection by raising the voltage above breakdown.

There are three basic types of quenching circuits: passive quenching, active quenching and gated quenching. There are also some combinations such as passive quenching with active reset, active quenching with passive reset, gated active quenching and passive gated quenching [43].

To analyze the quenching process easier, the simple equivalent circuit for APD is shown in Figure 2.1 [43] [44]. The mentioned model indicates the functionality of APD and is used to predict the reaction of the quench circuit when connected to the design quench circuit. The onset of an avalanche is modeled by turning on the switch. C_d stands for the depletion region's capacitance and R_d corresponds to the equivalent resistance, typically a few hundred Ohms. In the model, breakdown voltage is represented by V_{br}.

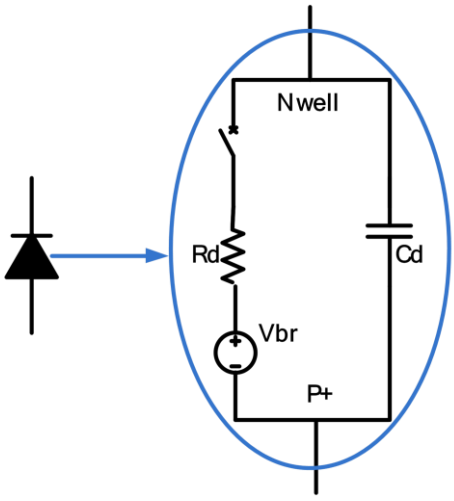

Figure 2.1: APD equivalent model

2.1.1 Passive Quenching

By observing the generation of single-photon pulses in the avalanche photodiodes biased above breakdown, APD is used in different applications such as astronomy and medical imaging. However, these applications were limited by the features of the device and quenching circuit. The first quenching circuit introduced was passive quenching.

The passive quenching circuit consists of a large resistor (R_L) connected in series with an APD. Subsequently the applied operating bias voltage is divided over the resistor and the APD. When there is minimal current, the voltage drop across the resistor is similarly minimal. Figure 2.2 illustrates a passive quenching scheme; the APD is sandwiched between R_L and a series resistor (R_S), where $R_S << R_L$. R_S is typically 50 to 100 Ohms while R_L is approximately 100K to 10M Ohms. The APD is connected to a power supply through R_L and R_S; the power supply biases the APD above the breakdown voltage. Capacitance C_P, which is sum of the stay capacitance (C_S) and depletion region capacitance (C_d) is initially charged to a bias voltage V_{Bias}.

When the APD triggers an avalanche and generates a large current, the current quickly discharges C_d and C_S and the voltage drops across the resistor R_L; as the result of lowering the voltage on the device, the avalanche current reduces. Quenching has occurred when the avalanche process is no longer self-sustaining, which means the diode current drops below the threshold. This threshold is called latching current (I_q) and it is in the range of 10 to 100 µA. The latching current forces the maximum avalanche current (I_f) to be equal or smaller than the latching current and the minimum voltage of the diode to be slightly more than the breakdown voltage and approximately equal to $V_{Br} + I_f R_d$ [43].

As soon as the current is quenched, C_P (sum of C_S and C_d) is recharged slowly by the sink current through load resistor R_L. The device recharges slowly and the APD voltage recovers toward the bias voltage exponentially to get the desired over-voltage with the time constant of $R_L C_P$; Thus, the device is ready for subsequent detection. R_L should be large enough so that the maximum avalanche current, which is equal to V_{ex} / R_L , is smaller than latching current. As a result of large resistance, the recharging time, called dead-time period, is very long and the maximum operating frequency is limited.

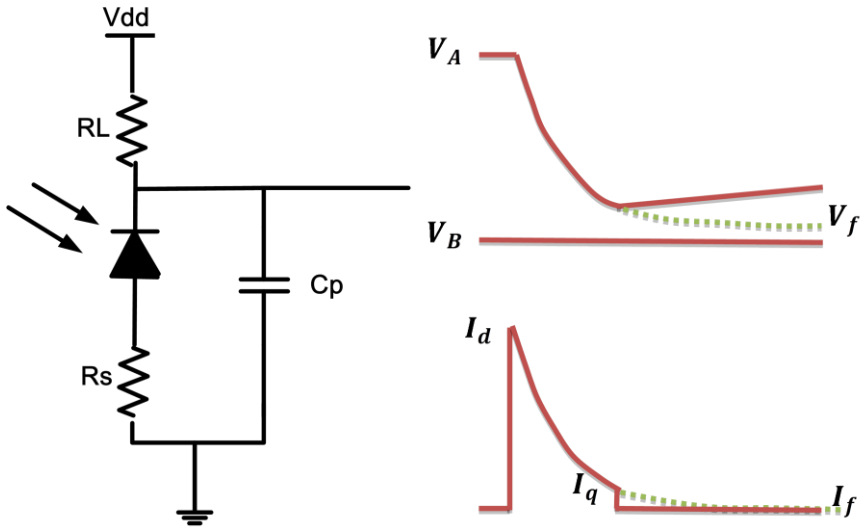

(a) (b)

Figure 2.2: Passive Quenching: (a) Circuit, (b) Avalanche voltage and current behaviour

A photon that arrives during the recovery time is almost certainly lost, because the avalanche triggering probability is very low during that time interval. Due to the slow recovery transient, passively-quenched device is not a good choice for high counting rate applications. Rather than long quenching time, after-pulsing and non-uniform bias voltage are additional disadvantages of passively-quenched device. As a consequence of long recharging time, an avalanche can be triggered before recharging is complete [43].

While the quenching process is relatively fast, the discharge of the current through the large resistance is quite slow and therefore the dead-time between photon sensing of passively-quenched device is estimated by device capacitance, stray capacitance, and device resistance. Dead-time (T_D) depends on total avalanche charge (Q_{PQ}) and final avalanche current (I_f). The total charge flowing through the device during avalanche in a passively-quenched device can be calculated by $V_{ex}(C_d + C_s)$. The current through APD is calculated by:

$$I_A(t) = \frac{V_d(t) - V_{Br}}{R_d} \tag{2-1}$$

$V_d(t)$ decreases exponentially, due to discharge of diode capacitor and stay capacitor, until the steady state occurs. The final avalanche current can be estimated by:

$$I_f = \frac{V_{Bias} - V_{Br}}{R_d + R_L} \tag{2-2}$$

Since $R_d \ll R_L$, the peak avalanche current is approximately equal to

$$I_f = \frac{V_{Ex}}{R_L} \tag{2-3}$$

To estimate the value of R_L resistance, equation (2-3) is used. To assure that the avalanche is quenched, the rule-of-thumb for a latching current, which ensures avalanche termination can be used. This rule is considered the maximum avalanche current, or final current, to be 100 μA or less [43] [45]. By knowing the required V_{ex} and assuming I_f to be 100 μA, the required R_L is calculated. Equation (2-4) is used to assess the quenching time for passive quenching.

$$T_D = \frac{Q_{PQ}}{I_{AP}} = R_L(C_d + C_S) \tag{2-4}$$

The quenching time for passive quenching is limited by the capacitance value of $(C_d + C_S)$ and is usually in the range of tens of nanoseconds (or 10^{-8}s). With an estimated 0.1 pF for a 20 μm radius APD and a 1 MΩ quenching resistor, the time constant is on the order of 100 nanoseconds. Additionally, it is typically difficult to reliably create uniform resistors, due to process variation and mismatching.

The avalanche current discharge C_S follows through R_S, and induces a voltage in the output. The avalanche signal depends on C_S/C_d. A stronger signal results in a larger ratio of C_S to C_d. An external capacitor in parallel to APD would also increase the avalanche signal; this method can be used when the diode capacitor is larger than stray capacitor.

If the interval between photon arrivals is shorter than T_D, the avalanche initiation probability, and consequently the detection efficiency will vary with time. This is highly undesirable. In addition, the output pulse amplitudes will also vary, and therefore some pulses may be missed by the sensing circuitry; because most sampling circuits have a constant amplitude threshold [46] [47]. Since R_L is determined by the latching current and C_d is an artifact of the junction itself, the only way to reduce T_Q in a passively-quenched device is by reducing the stay capacitance. The most effective way of doing this is by integrating the quenching resistor on the same die as the APD itself [48] [49].

The performance of a passively-quenched device may be affected by the choice of the resistor element. An off-chip resistor can have highly-precise resistance but will add parasitic capacitance. On-chip resistors typically have very high temperature coefficients and take up large areas. Transistors are a good choice but require a high-quality CMOS process and clean voltage supplies. Moreover, they are limited by the supply voltage V_{DD} of the specific technology. This sets a limit on the allowed excess voltage with which APD can operate and influence the physical design of the unit.

2.1.2 Active Quenching

A solution to the drawbacks of passive quenching due to long recovery time is to reduce the stray capacitance Cs and so as to make the recovery time shorter. In the case of Cs being in the order of few pF (10^{-12} Farad) the recovery time is below micro seconds which is a desirable design characteristic for applications with lower counting rate requirement. However, for high counting rates (>10^6 counts per second), the passive quenching is still not applicable. In 1975, the active quenching was introduced and commercialized by Cova and colleagues [37] [50]. Active quenching circuit was introduced as a feedback loop to lower bias voltage on the device when the avalanche event is detected. Besides being more complex circuits, active quenching circuits were introduced to overcome the difficulties of passive quenching and recharging [43] [51] [52] and several configurations and schemes were contributed by various laboratories [53] [54].

In active quenching, active recharging scheme is more common; since complete quenching can be achieved via a high resistor while the faster recharge can be attained by replacing R_L by a smaller resistor. Therefore, two resistors are used (one for quenching and one for recharge) and a switching circuit to switch between them. Analog circuitry senses the onset of an avalanche and then disconnects the quenching resistor and connects the smaller recharge resistor. Another circuit senses the completion of the recharge process and quickly disconnects the smaller resistor and reconnects the quenching resistor. An example of this circuit is shown in Figure 2.3 [55] [56]. The device is biased above the breakdown voltage as in the passive-quenched device. When the device is in the detection state, switch S1 and S2 are turned off (i.e. in open position). As an avalanche event is triggered, the current induces a voltage change on R_S that is detected by a comparator. After a short delay due to feedback loop, switch S1 is turned on (i.e. in close position). Turning on switch S1 results in raising the anode voltage quickly to V_Q, and lowering

the voltage across APD to V_A-V_Q, which is a few volts lower than the breakdown voltage. After a certain hold-off time, which can be preset by M2, switch S2 is turned on (i.e. in close position) for a short time to quickly recharge the device and enable it for subsequent detection. The inherent risk in this scheme is the arrival of a photon after recharging is full or almost complete, but before the disconnection of the recharging resistor. This results in an avalanche which is not quenched [57].

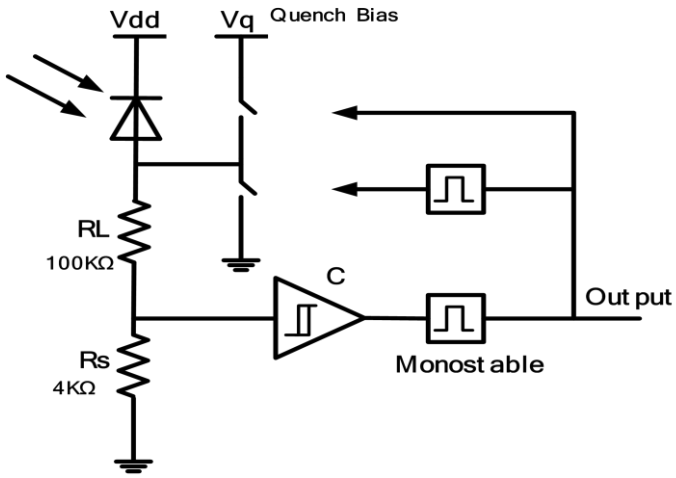

Figure 2.3: Active Quenching Circuit Concept

In an active quenching scheme, an external circuit senses the onset of an avalanche. For example, a comparator may sense a voltage drop, and quickly trigger a reduction in the APD voltage to a level below the breakdown of the device [57]. While active quenching schemes can be effective in large and slow APDs, it has some limitations in the case of high over bias voltage [45] or small junction capacitance [58].

A basic active quenching circuit is illustrated in Figure 2.4 [28]. The two main sub-circuits are a comparator and a voltage driver. The comparator is used to detect the avalanche rise for photon counting or timing. The output pulse from comparator must be shaped to be processed by signal processing circuitry. Generally a line driver is used to boost the amplitude of this pulse before sending it to appropriate circuitry for counting the detected photon. The comparator also sends a command to the voltage driver which is then used to lower the bias voltage but still above the breakdown voltage of the APD. After a precisely controlled hold-off time is passed, the bias voltage is restored back to the voltage which is below breakdown and the APD becomes

ready to detect the next photon. At this point, one quenching cycle is completed. The active loop can complete the task after loop delay by forcing the APD voltage well above the breakdown voltage, with sufficient margin to ensure final quenching and avoid registration that is due to non-uniformity of breakdown voltage over the APD active area. The active loop also forces a fast reset transition and makes it possible to introduce a controlled hold-off time. By minimizing the pulse charge, trapping and APD power dissipation can be minimized.

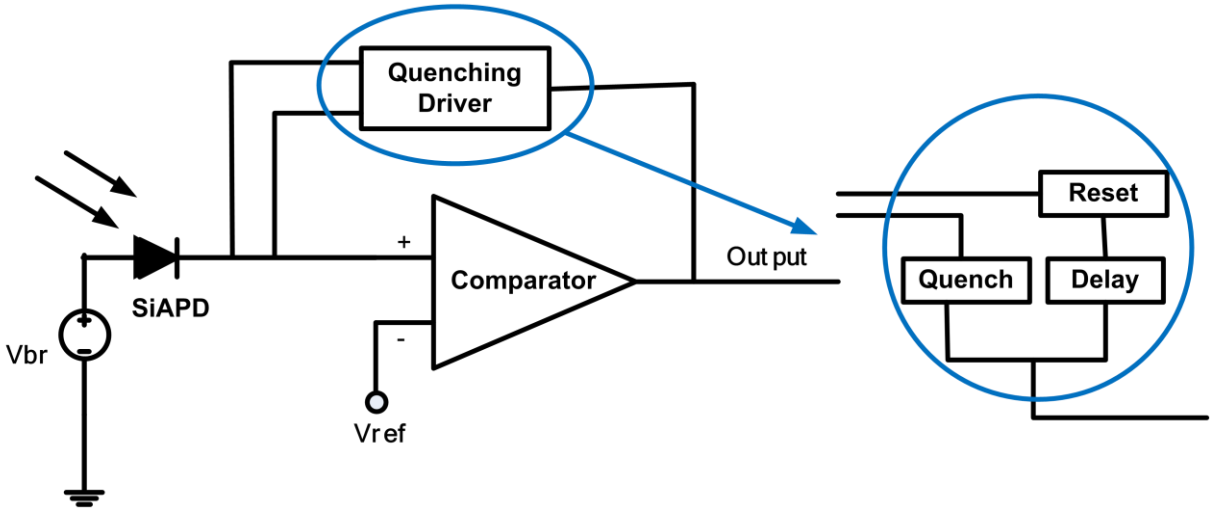

Figure 2.4: Active Quenching Circuit

The quenching time is the sum of circulation time in the feedback loop and the rise time of the quenching pulse [43]. As quenching voltage (V_Q) decreases, the rise time and therefore quenching time decreases.

Compared to a passively-quenched device, an actively-quenched APD has several advantages. In an actively-quenched APD, the delay between the onset of an avalanche and the time it is recharged can be controlled. This is desirable in terms of device noise, and especially after-pulsing. In addition, well-defined on and off voltages, adjustable hold-off time, and fast reset are the advantages of actively-quench device. These desirable characteristics are independent of the physical characteristics of under-test APD. Due to these advantages, active quenching circuits have replaced passive quenching circuits in many applications. However, the main disadvantage of present active-recharge-quenching scheme is its larger size and higher power consumption.

2.1.3 Further improvement

Next generation of quenching circuits are mixed quenching circuits, which are a combination of passive and active quenching. The mixed quenching circuits provide flexibility in the choice of the passive load. Since a quasi-quenching action is sufficient, load resistance R_L can be smaller than the minimum value required for passive quenching. An inductive load can also be employed to enhance the reduction of the avalanche current for a short time, covering the delay of the active feedback loop. However, to obtain satisfactory results and avoid overshoots and instability that is due to the unavoidable combination of inductance and capacitances, such a circuit must be accurately analyzed and carefully implemented.

On the other hand, the overall performance of a single photon detection system not only depends on the APD characteristics but also on peripheral circuits, including quenching circuit and the temperature control system. For example, the dead-time of a quenching circuit determines the total charge flowing through the device during avalanche which affects after-pulsing characteristics [59]. In addition, as the thermal effect was studied in section 1.2.3.7, having an on-chip control system which can control the thermal effect is necessary.

2.1.4 Thermal Effect Control

As a result of increase in temperature, the breakdown voltage becomes higher, the diode noise increases rapidly, and the gain decreases. Therefore it is important to cool the system. The implications of the system without cooler are twofold: (a) by increase in temperature, the avalanche voltage increases and differs from the initial voltage; therefore, the operation mode of APD may change and there is no guarantee that APD can continue working in the single photon detection mode. (b) As mentioned in section 1.2.3.7, an increase in temperature results in APD breakdown voltage (V_{Br}) increase. This means that, by keeping the bias voltage constant, the excess voltage (V_{ex}) may not be the optimum value anymore, and the single photon detection efficiency may drop. (c) As discussed in section 1.2.3.4, an increase in temperature causes rapid increase in thermal noise. By increase in the noise level, the amplitude of the detected pulse in the output may increase as a result of thermal carriers. This may cause interference in the accuracy of photon counting. (d) APD gain in both linear and Gieger modes of operation is another parameter that would decrease by an increase in temperature.

Consequently, different methods are suggested for cooling APDs. A common suggested solution is using fluid nitrogen or thermo-electricity cooling [60] [61] [62]. The simplicity of structure makes thermo-electronic cooling system become a conventional solution for APDs. However, since they have high power-consumption and are not integrated, APDs with thermo-electronic coolers have to be used in laboratory settings [63], or in large instruments, where the power consumption is not a limitation. Another solution is to design a control algorithm to compensate for the thermal effect on APD parameters such as noise, gain, efficiency and SNR. This method is a suitable solution for integrated devices. In most of suggested solutions, designing a temperature-independent technique for automatic regulation of bias voltage is essential. This technique results in maintaining the optimum excess voltage unchanged. The following algorithms present some examples of compensation methods discussed in the literature:

The first method concerns the monitoring of noise changes [64]. This method is based on the rapid increase of noise as a result of temperature increase. A signal is detected as the output of noise change, and then is amplified and measured. When the detected noise voltage exceeds a certain range, the bias voltage is decreased; and vice-versa, when noise signal decreases, the bias voltage is increased. In this method the noise character nearby avalanche is studied, and the bias voltage is stabilized based on noise characteristics [64].

Another method considers constant excess voltage, where the bias voltage is controlled as a function of the variation of breakdown voltage due to the change of temperature. In this method there is a temperature-breakdown voltage lookup table stored in a memory and the appropriate bias voltage is selected from the values in the lookup table [65]. Since breakdown voltage has a linear relation with temperature (over the operating range) the temperature coefficient is defined as an APD specification and it can be replaced by the lookup table [66]. In this method, a reference voltage is set to be a voltage implementing an optimal amplification ratio on an output terminal; the desired voltage is generated by considering the slope variation of the plot of temperature and breakdown voltage. To verify the suitable bias voltage used to compensate the effect of temperature, there are two possibilities for the input of control loop: first input can be from a temperature sensor, while the second possible input can be the amplitude of the APD terminal output [66].

The third method is to use two APDs to eliminate the effect of noise on gain calculation and define a multiplication factor as:

$$M_{ph} = \frac{I_M}{I_P} \tag{2-5}$$

where I_M is the un-multiplied current of the APD biased at high gain and I_P is the primary un-multiplied current of the APD at low gain.

By changing the bias voltage of a high-gain device, while maintaining a constant bias on low-gain APD, the current ratio, and hence the high-gain of the device can be set at pre-selected values [67]. From the ideal diode equation, the effect of temperature change on the low-gain device is negligible when compared to the large-gain effect on the device. Therefore, over moderate changes in room temperature I_P remains constant while I_M varies. In this method the circuit is monitored to maintain its preset gain by adjusting the bias voltage of the high-gain device [67].

CHAPTER 3 QUENCH-RESET CIRCUIT: SIMULATION AND POST LAYOUT RESULT

3.1 Design Procedure

As mentioned in section 1.3, the drawback of APD operating in Geiger-mode is that the avalanche self-sustaining process continues until it is stopped externally. Due to the need for an external stop and consequent quick reduction of the bias voltage, a quench-reset circuit must be employed. The idea is to keep the APD in a sensitive condition, which is 1 volt above the breakdown voltage for our case. As a result, by absorbing a photon and triggering an avalanche, an increase of 400μA in output current occurs and therefore the APD cathode voltage would increase by 1.5V. At this point the quench-reset circuit should be active to quench the avalanche and return the APD to a sensitive state. When the avalanche is quenched the current is reset to zero, and the voltage slowly returns to its value before detecting a photon (i.e., sensitive value). The block diagram of the proposed solution is depicted in Figure 3.1. The Geiger-mode front-end circuit is activated by sensing the leading edge of APD cathode voltage as a result of the avalanche current. The quench block suppresses the avalanche current by lowering the bias voltage below the critical value which may be very close to the junction breakdown voltage of the semiconductor.

The output of the quenching block is digitized to be sent to the counter to complete the photon detection system by measuring the time interval between successive pulses. After the pulse is generated, the APD should be rearmed for subsequent detection; this is where the reset block can be employed to bring back the APD voltage to the original sensitive level.

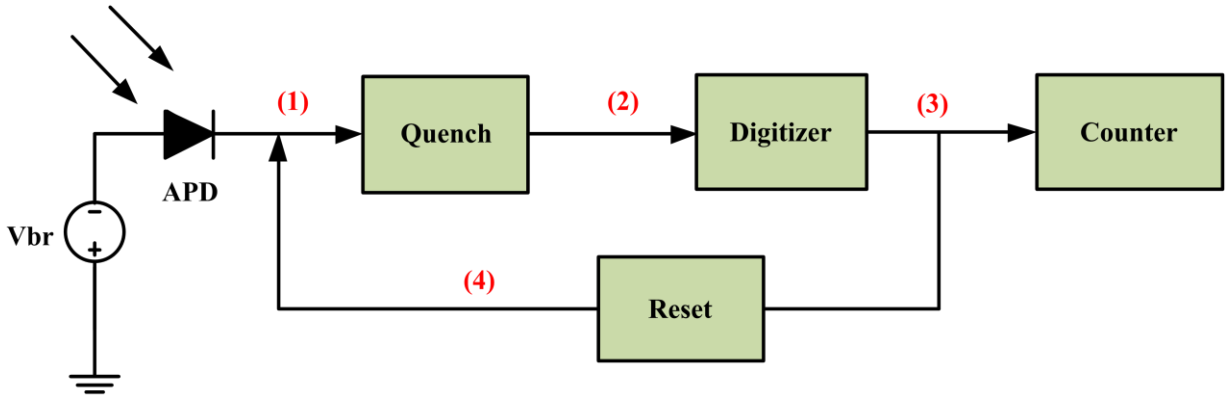

(a)

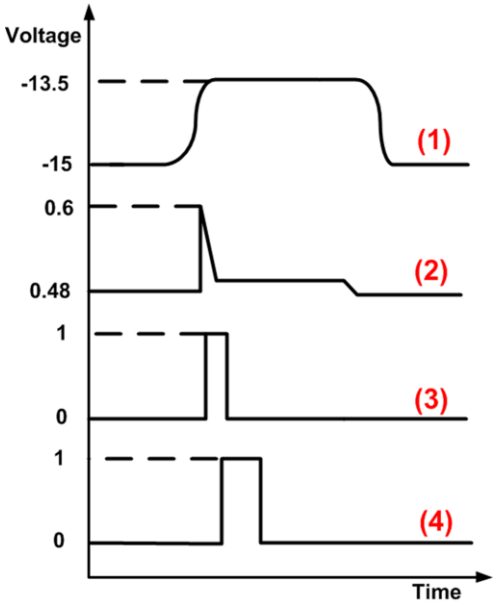

Design Specification:

- ✓ Dead-time T_D <20 ns
- ✓ Controllable reset time (1ns<T_R<2µs)
- ✓ Power consumption <10 µW
- ✓ Integrated

(b)

Figure 3.1: Quench-Reset Overall: (a) system level block diagram, (b) expected signal

The proposed quench-reset mechanism is depicted in Figure 3.2. Figure 3.2a illustrates the circuit which is responsible for quenching while Figure 3.2b demonstrates the reset circuit. Figure 3.2c shows an inverter which is responsible for digitizing the pulse related to detected photon and sending it to reset circuit and counter circuit. Figure 3.2d is a 5-bit asynchronous counter to keep track of the number of detected photons. The counter is composed of 5 D-flip flops.

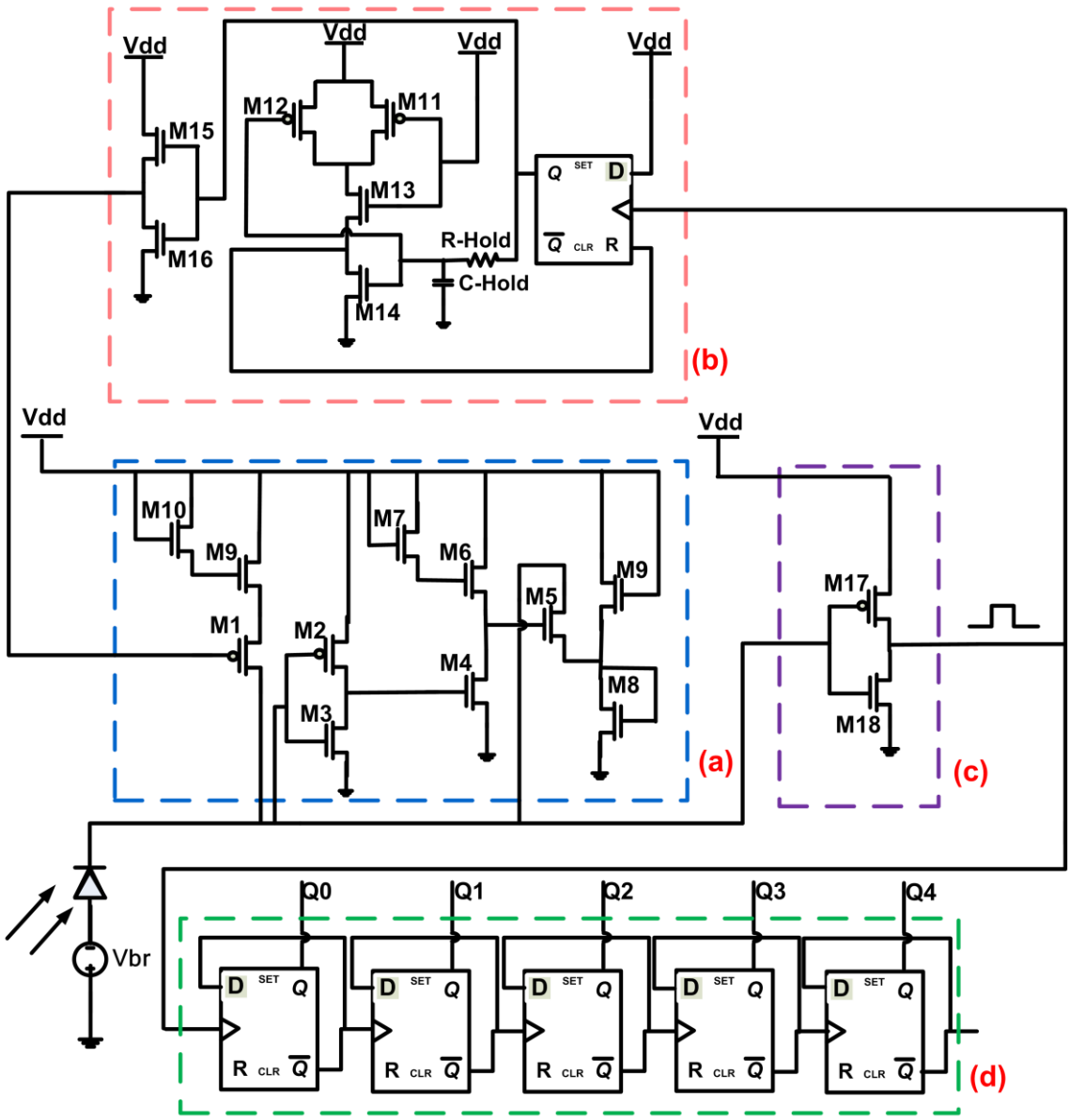

Figure 3.2: Circuit level design: (a) Quench Circuit, (b) Reset Circuit, (c) Digitizer, (d) Counter

Figure 3.3a illustrates the quench circuit which consists of a level shifter and a quencher. The APD cathode voltage, which is the input to the quench circuit, as shown in Figure 3.3b, is not in the operating range for transistors. Therefore, the first section of the quench circuit works as a level shifter, which consists of M1, its load M9 and M10 as provider of self adjusting bias to the load M9. The pulse to activate switch M1 comes from the reset block, which will be described

later. Figure 3.3c indicates the level-shifter output. The level shifter block is capable of shifting the APD cathode voltage signal from the range between -15V and -14.2V to the range between 480mV and 600mV.

The quencher block in Figure 3.3a is responsible for quenching the avalanche current. On influx of photons, the avalanche raises the voltage across APD. At this moment, transistor M4, which is biased in common source (CS) mode, amplifies the signal. As the output of M4 increases, it turns on transistor M5, and the quench process occurs by lowering the APD voltage by M5. The quencher output is shown in Figure 3.3d. As the quenching process is faster and the quenching time is lower, the power loss and therefore the heating would be less.

Figure 3.4 indicates the functionality of the digitizer block which is an inverter. It is responsible to digitize the output of quench circuit and prepare it for reset and counter circuits. Figure 3.4a and Figure 3.4c shows the input and the output of the inverter, respectively.

Figure 3.5a illustrates the reset circuit which consists of four main blocks of a D-flip flop, hold-off RC, a NAND gate and a buffer. The enable pulse from the digitizer is detected by D-flip flop which is sensitive to rising edge. The RC hold-off holds the APD cathode voltage in its existing voltage level for the hold-off period with respect to the value of the resistor R-Hold and the capacitor C-Hold. Hold-off RC, NAND gate and buffer constitute monostable block and generate the signal to recharge the APD back to its operation level by activating switch M1 in quench circuit, as presented in Figure 3.6. The low resistance transistor M1 resets the quiescent bias of the APD and brings the APD cathode voltage back to its operative level for detecting the next photon arrival. Figure 3.5b and Figure 3.5c show the input and the output signals of the reset circuit, respectively.

The reset process should be as fast as possible to avoid dark current noise. The reset time for the designed circuit is in the range of 1 to 3 ns, while the quenching time is 1 to 4 ns. The most suitable value for hold-off time is unique for each system and it depends on the nature, density and lifetime of the traps of each specific APD. It should be long enough to allow trapped carriers to be emitted and not to allow the after-pulsing affect the photon counting statistics. On the other hand, hold-off time should not be too long to avoid limiting the repetition rate and affecting the validity of the counting statistics. For our circuit, the hold-off time is controllable in the range of 4ns to 2μs.

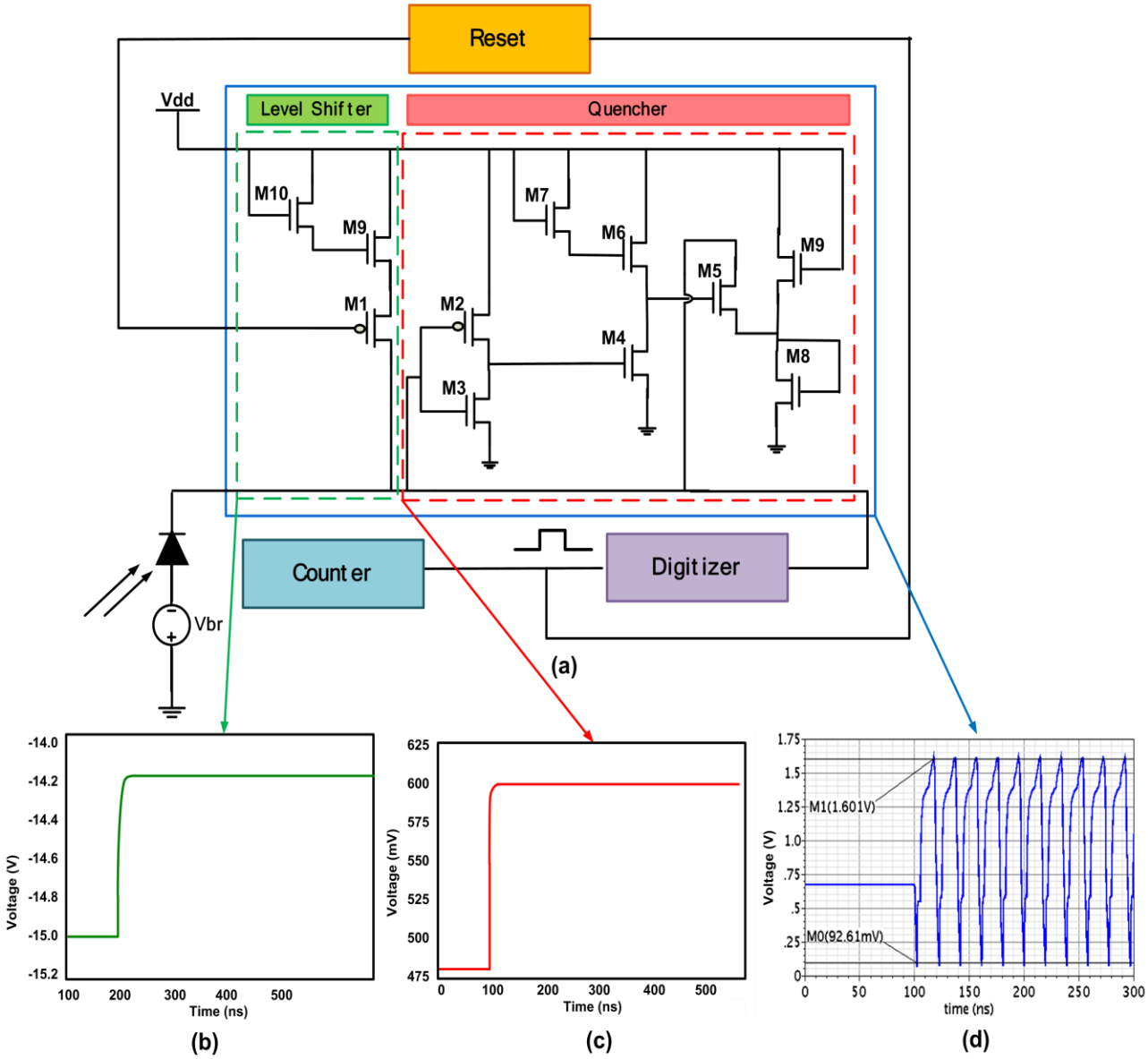

Figure 3.3: (a) The quench circuit which consists of a level shifter and a quencher, (b) APD cathode voltage in absence of the quench circuit, (c) Level shifter Output, (d) Quencher Output

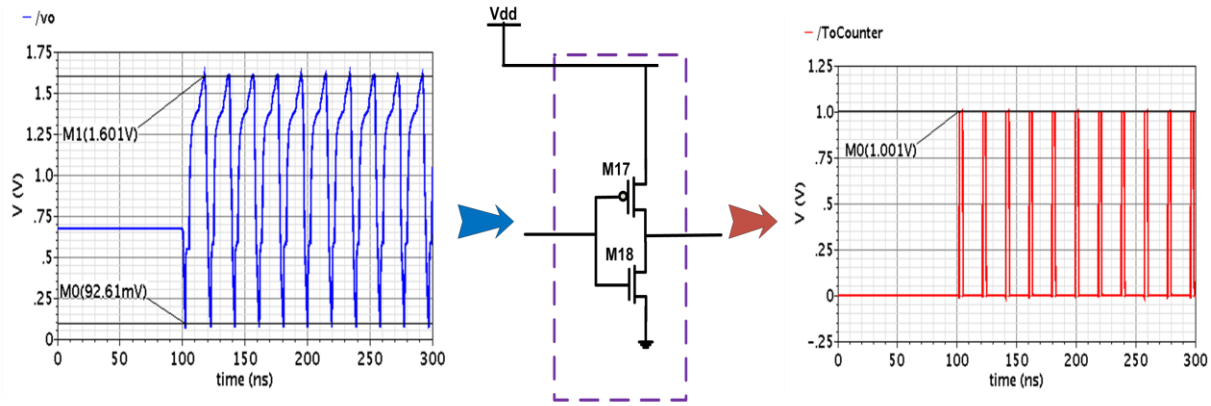

. (a) (b) (C)

Figure 3.4: The functionality of digitizer block: (a) Input Signal, (b) Digitizer block, (c) Output Signal

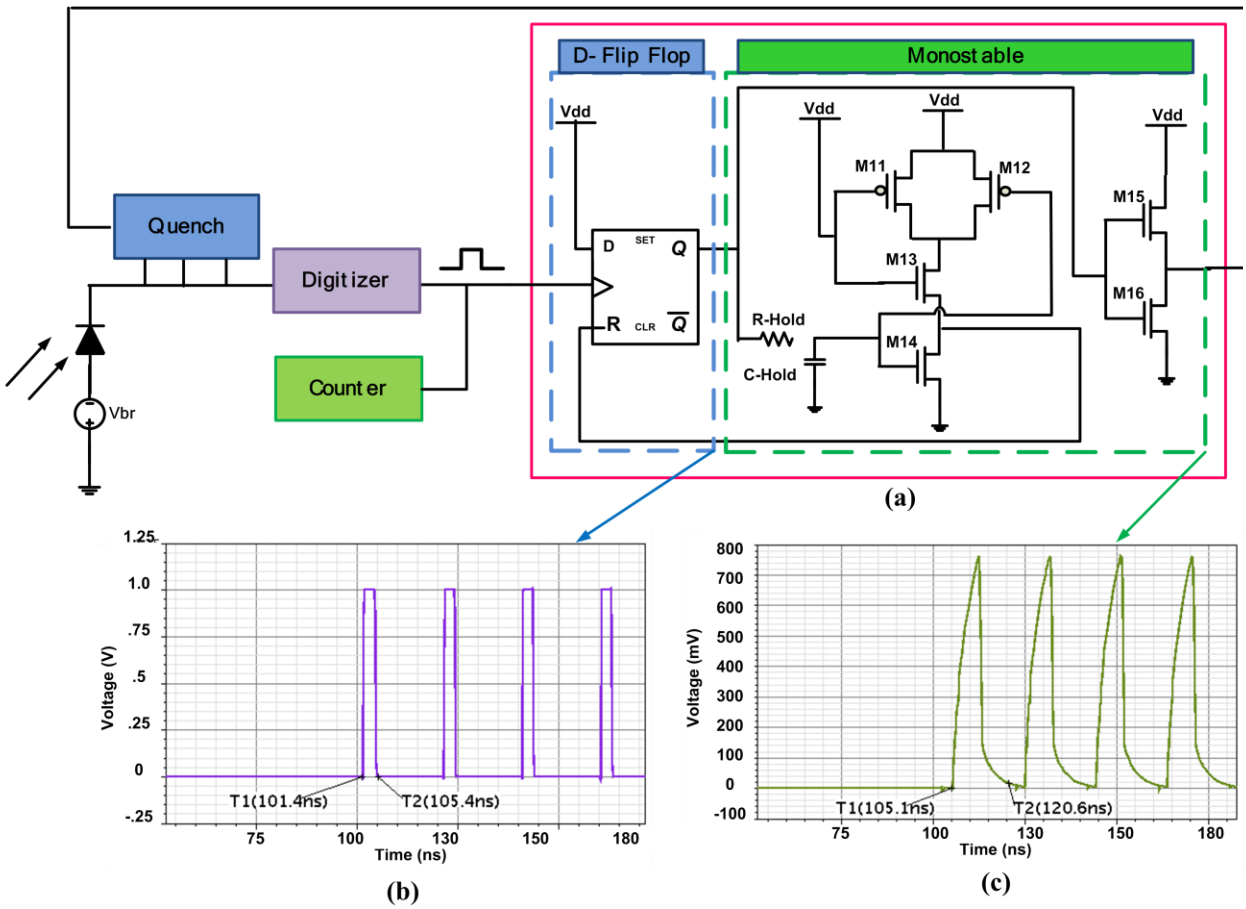

Figure 3.5: The functionality of reset block : (a) Circuit design, (b) Detected signal by D-flip flop, (c) generated enable signal for Quench circuit

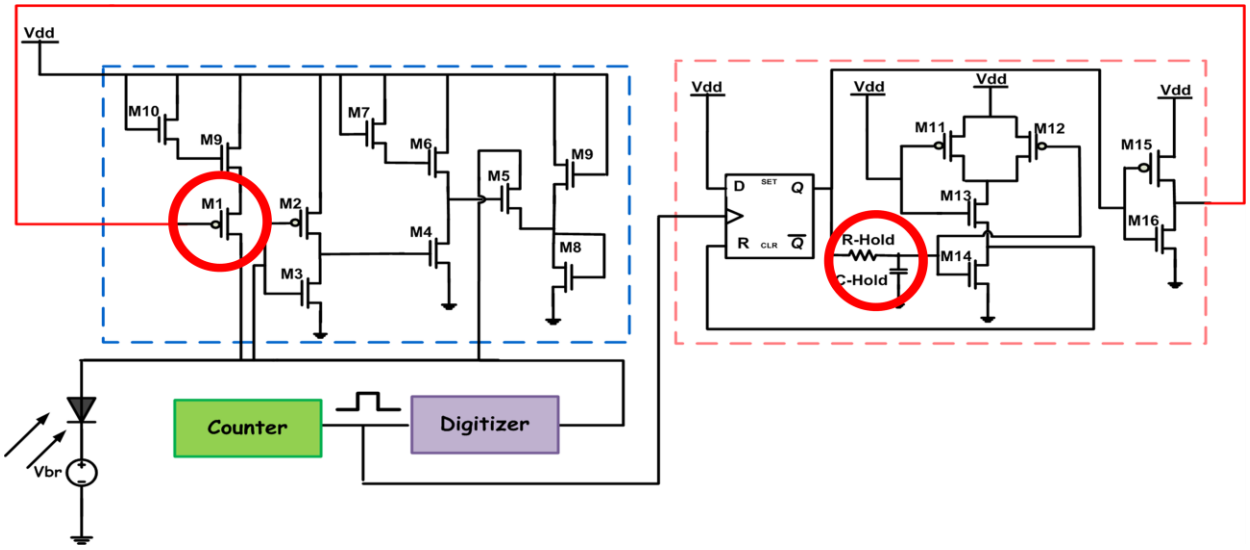

Figure 3.6: The feedback path of reset block

3.2 Simulation Result

The proposed circuit was simulated using the Cadence and Virtuoso layout editor and was implemented in 180nm standard CMOS technology. To simulate the circuit, an APD model was designed as demonstrated in Figure 3.7. The model was designed based on bulk contact resistance (R), parasitic resistance (r), junction capacitance (C), and breakdown voltage of wirebond inductance and bondpad capacitance are neglected. The model was designed to simulate the performance of an APD which is being designed by our research group. Therefore the breakdown voltage was chosen as 15V, and the chosen values for R, r, and C were 2kΩ, 1kΩ, and 1pF, respectively. Current source I in the model is mimicking the avalanche triggering. To test the sensitivity of the proposed circuit to low excess voltage, the amplitude value of the current source is chosen to be 350μA to have the excess voltage of 0.8 V.

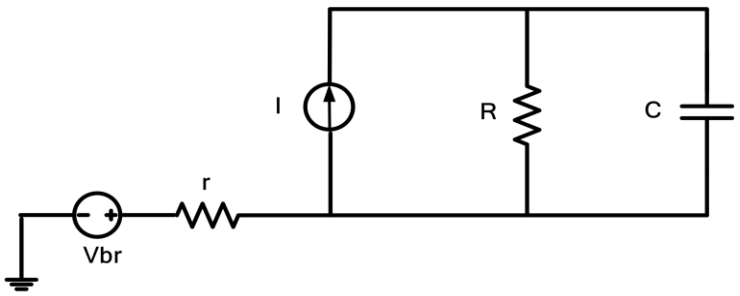

Figure 3.7: APD simulation model

3.2.1 Schematics

To lower the cost and reduce the design size, the design would greatly benefit from computer-aided-design (CAD) tools that would allow optimization and verification of a particular system before its actual fabrication. A transistor-levels design was first created as a schematic in Cadence's 'Schematic Editor' to verify the performance of the circuit.

To estimate the photon counting rate, dead-time needs to be calculated. Dead-time is the sum of quench time, hold-off time and reset time. Figure 3.8 indicates the performance of the APD cathode voltage, and the output voltage to the counter, when the hold-off time is zero. Figure 3.8a shows 3 cycles of light impinging, where signal demonstrates the light from LED; APD cathode voltage quenches during light impinging and for each quenching event, a pulse is generated in output voltage. Figure 3.8b, a diagrammatic representation of the results, conveys that there is a time constant of 0.5 ns for light impinging. The quenching occurs in 0.91 ns. The output voltage pulse is detected within 0.58 ns of the onset of the quenching. The width of the output voltage pulse is approximately 1ns and it ends in 1.58 ns after the light impinge.

Besides having fast quenching, it is important to ensure that the output pulses are not interfered by dark current. Therefore having controllable hold-off time is significant. Figure 3.9 illustrated the same signals when the hold-off time is defined as 13 ns. In Figure 3.9a, the blue signal shows the current occurred as a result of light impinging; the red signal and the green signal indicate APD cathode voltage and quench-reset output voltage respectively. The orange signal indicates the resetting pulse with the width equal to hold-off time value. Figure 3.9b is the zoomed-in version of Figure 3.9a, and indicates that the quenching occurs at 2.3 ns after detecting the light. However the reset pulse is generated 3ns later. This means that the design resetting feedback block creates 2.7 ns delay. The resetting pulse has the width of 13 ns, which indicates the hold-off time. When the resetting pulse disables, it takes 2.7ns for APD voltage to return to original voltage level and for the device to be rearmed for subsequent detection. This time is called reset time. The overall dead-time in this case is 20ns with 13ns pre-defined hold-off time.

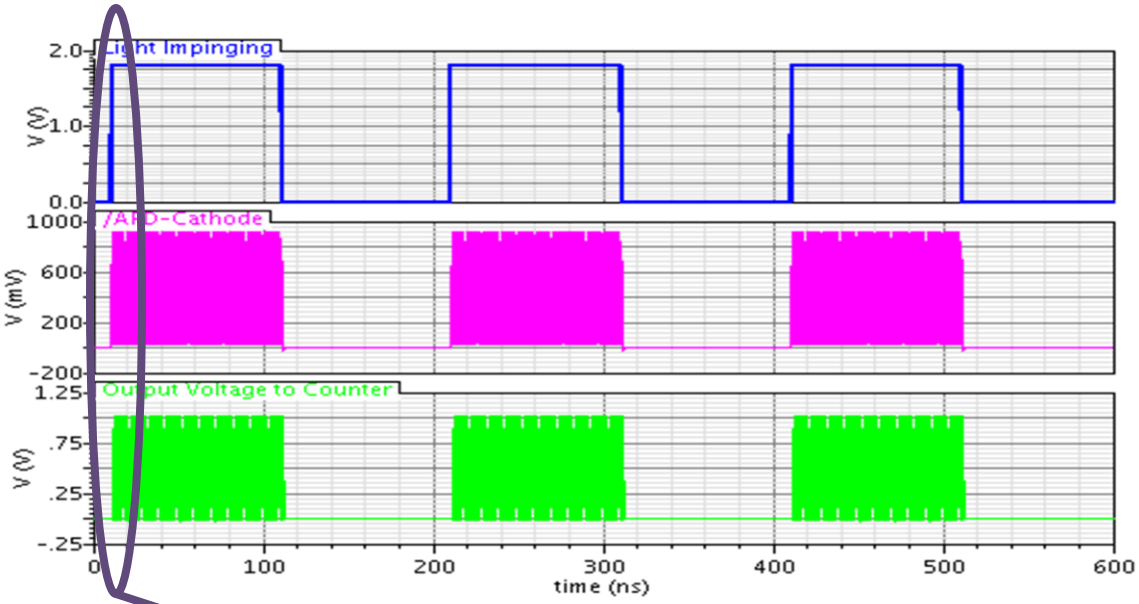

(a)

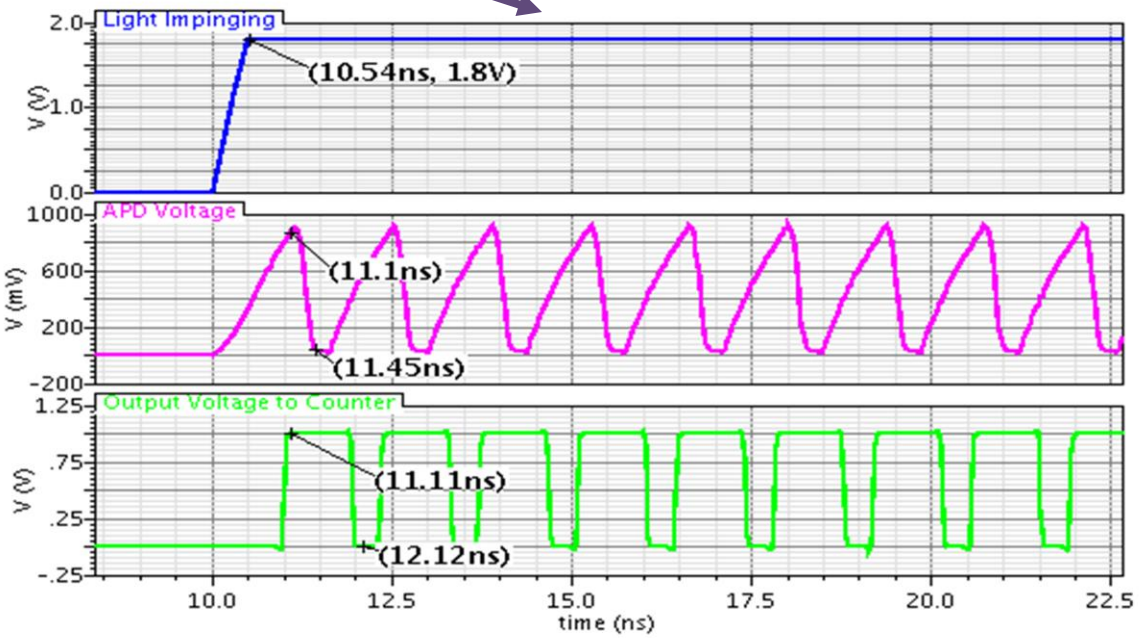

(b)

Figure 3.8: Schematic simulation of the quench-reset circuit with no hold-off in terms of APD voltage and output voltage: (a) 3 cycles of light emitting, (b) Zoom-in plot indicating quenching

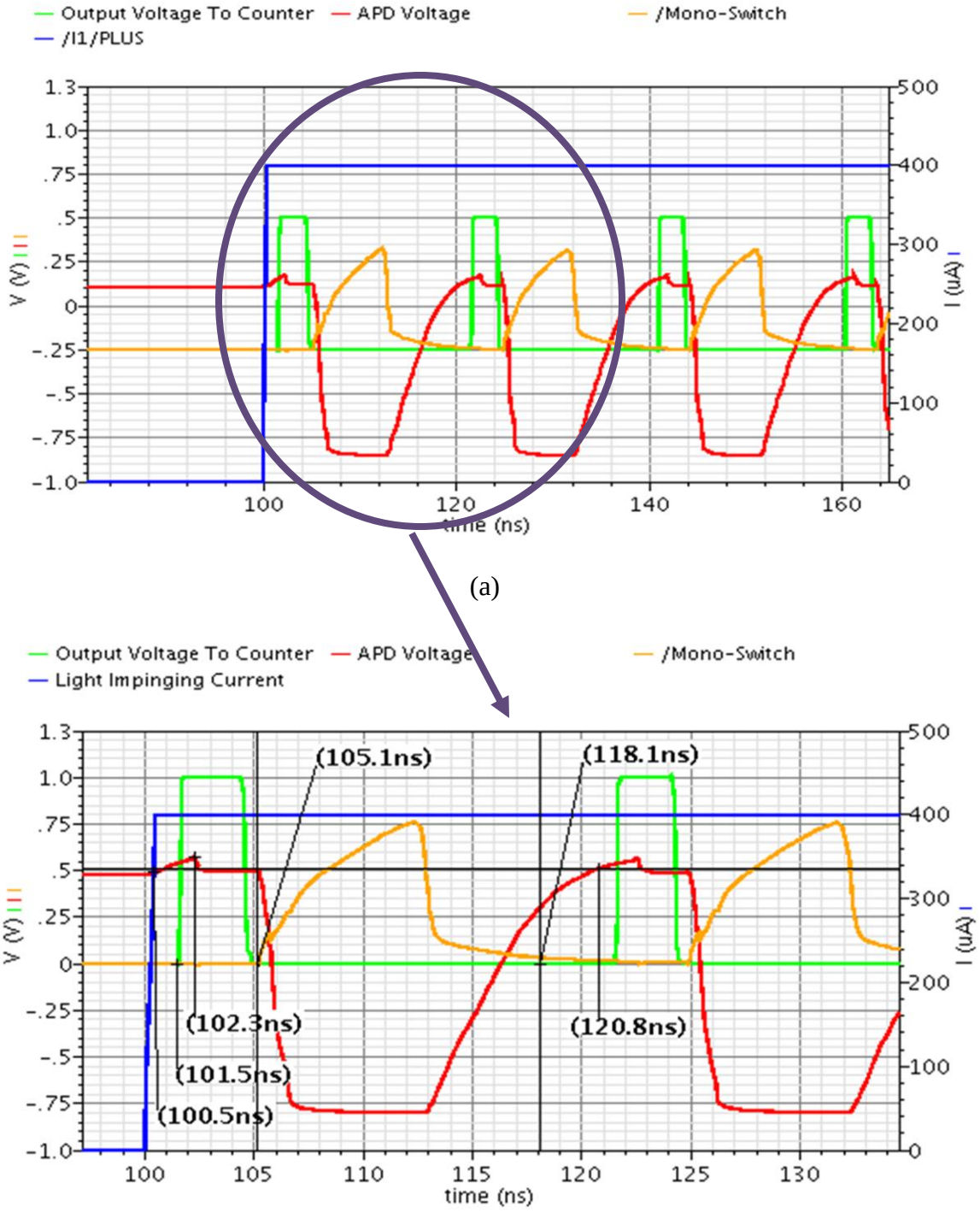

Figure 3.9: Schematic simulation of the quench-reset circuit with 13 ns hold-off showing APD voltage, output voltage and reset pulse: (a) 4 quenching cycles, (b) Zoom-in plot

3.2.2 Post-Layout

Once the performance parameters of the quench-reset circuitry were validated through simulations, the 'Virtuoso Layout Editor' tool from Cadence was used to create a compact layout design for this circuitry. After the layout was completed, Design Rule Checker (DRC) was used to make sure that all the shapes in the layout conformed to the design rules given in the design rule specification sheet for this CMOS technology. Once the layout cleared all the DRCs, a netlist check was performed using Layout-Versus-Schematic (LVS). LVS ensures that all the connections in the layout are correct and the netlist extracted from the layout matches the one extracted from the schematic. After the checks were cleared, the extraction tool was used to extract a netlist from the designed layout with all the parasitic resistors and capacitors annotated within. This new parasitic annotated netlist was then used to simulate and verify all significant parameters of the circuitry again.

In case a particular important value is different from the design value then the circuit layout has to be investigated and likely re-modified to fix this mismatch. Like all designs, such “re-work” can be anticipated. After some modification, the simulations of the extracted netlist were very close to the original schematic simulations and therefore no further modifications became necessary.

Figure 3.10 demonstrates the layout result of the APD voltage and output voltage of quench-reset circuitry with zero hold-off time. Figure 3.10b indicates that quenching occurred at 0.72 ns and the output voltage ended at 0.83 ns.

Several additional measurements were taken in order to ensure the fabrication success of the Quench-Reset design presented in this thesis. Figure 3.11 illustrates AC analysis of Quench-Reset circuitry in the frequency range of 100 Hz to 5 GHz. It shows that the bandwidth of the circuitry is 1.153 GHz.

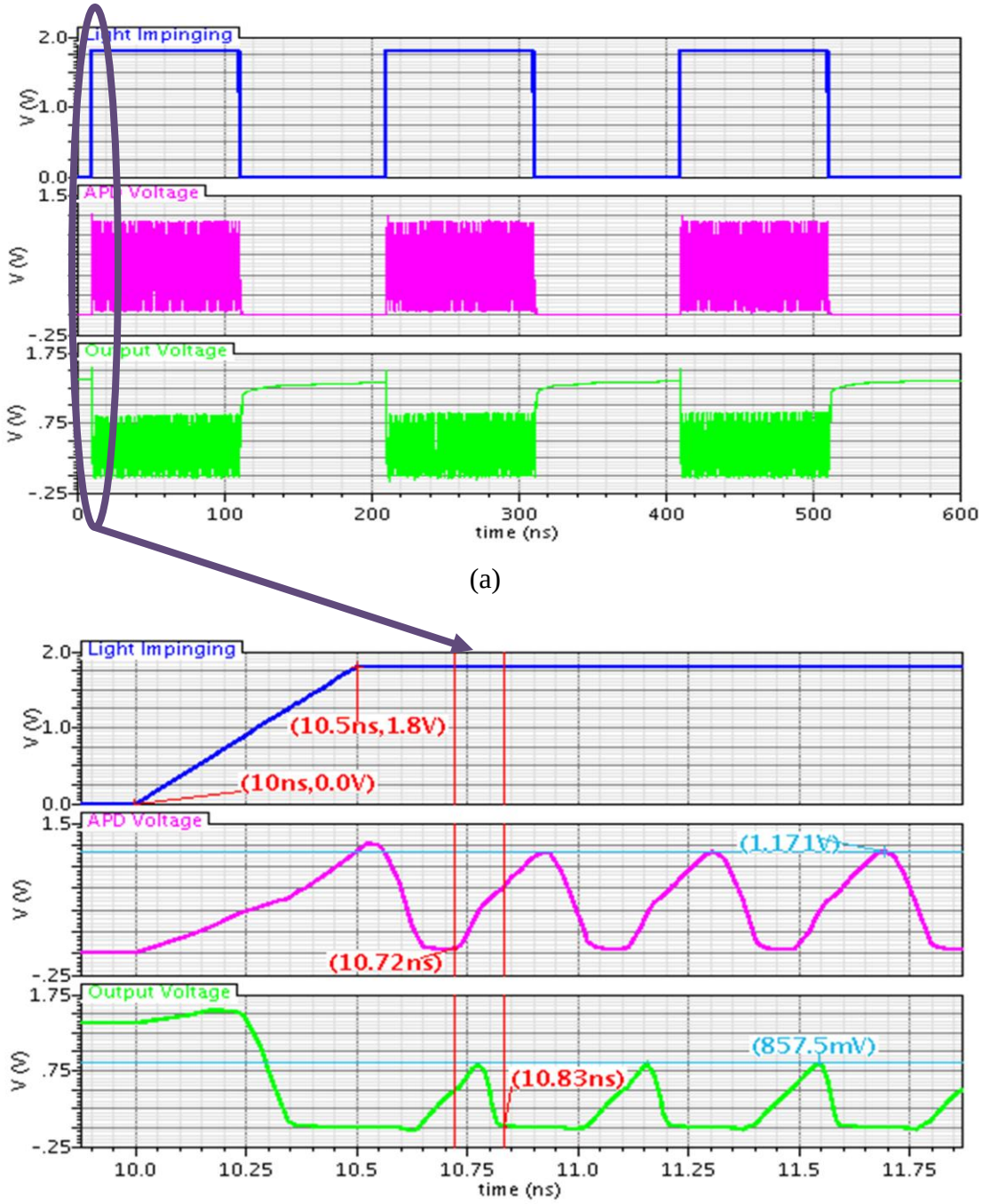

(a)

(b)

Figure 3.10: Layout simulation quench-reset circuit in term of APD voltage, output voltage and reset pulse: (a) 3 cycles of light emitting, (b) Zoom-in plot

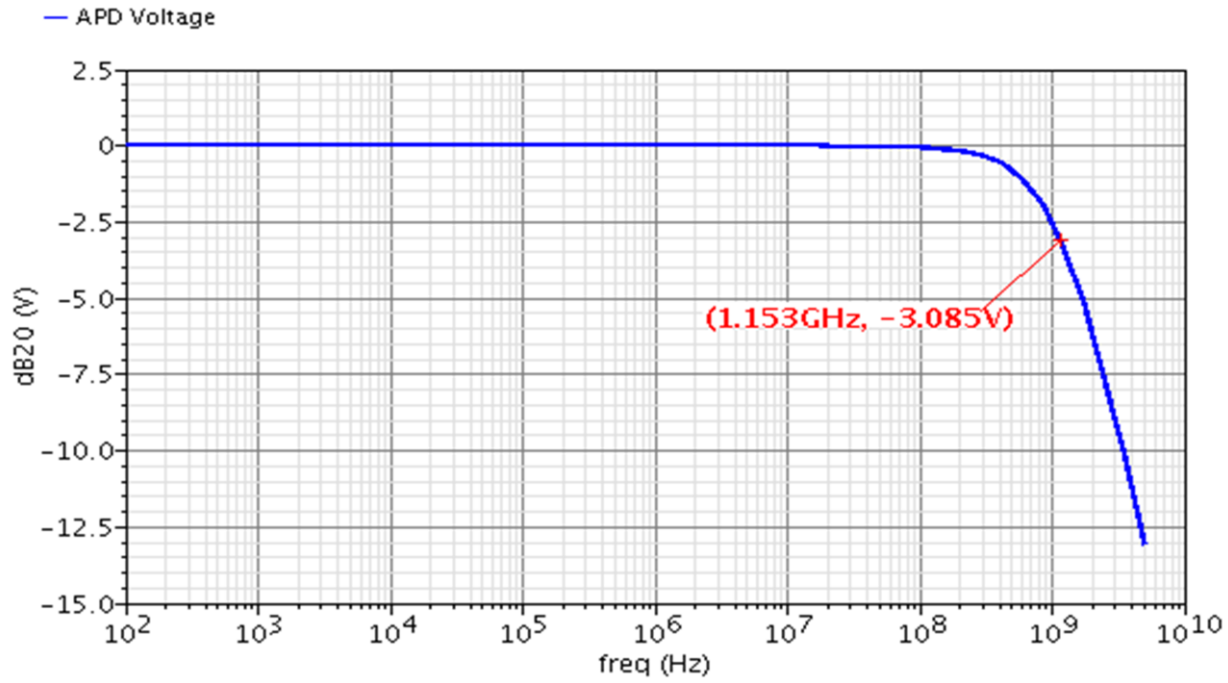

Figure 3.11: AC analysis of the Quench-Reset circuitry to estimate the bandwidth (BW)

3.3 Controller design for APD performance improvement

As explained in section 1.2.3.7, the thermal effect is the main bottleneck on the system performance. It affects the gain and signal-to-noise ratio (SNR) in both linear and Geiger modes. Figure 3.12 illustrates the system control algorithm to compensate the thermal effect. The trivial solution may be using a temperature sensor and a cooler which keep the temperature changes constant. However, to have the fully integrated system, the cooler should be avoided as a solution to compensate the thermal effect; instead we should find another parameter which affects on the gain and can compensates the thermal effect. In the following system two algorithms are proposed depending on the mode of operation, which is based on the relationship between bias and breakdown voltages. In Figure 3.12 the two thermal effect control algorithms of linear-mode and Geiger-mode are presented. In both algorithms the thermal effect is compensated by changing the bias voltage through Voltage Generator Section.

As mentioned in section 1.2.2, APD gain in linear mode can be calculated based on equation (3-1).

$$G = \frac{1}{1 - [\frac{V_{bias} - I \times R}{V_{br} + \gamma(T - T_0)}]^n} \quad (3\text{-}1)$$

where, I and R represent the total current and total equivalent resistance of APD. T_0 is room temperature at 25℃, T is the instant temperature and γ is a temperature coefficient. n is determined by the character of the semiconductor material which is used to make the APD, and its value ranges between 2 and 7 [68].

V_{br} is changing linearly with temperature and γ indicate the changes of voltage per each Celsius degree of change in temperature. V_{ir}, which is the equivalent voltage of $I \times R$ in equation (3-1), is very small when compared with V_{bias}. Therefore a good estimation for the new required V_{bias} is to apply the changes on breakdown voltage through temperature coefficient to primary bias voltage. Figure 3.12a shows the methodology to compensate the thermal effect in linear mode. The physical parameters of APD: γ and n along with initial temperature (T_0) are preset. By storing the initial values, the gain at initial temperature is calculated. By monitoring room temperature the expected change in breakdown voltage can be calculated through preset temperature coefficient. Thus, the calculated new value for bias voltage would be sent to voltage generator section. By calculating new gain based on new bias voltage and new breakdown voltage, the difference between the new gain and default gain is estimated and the accuracy of this algorithm can be judged.

Similar methodology is used for Geiger mode. The gain in calculated through equation (3-2).

$$G = \frac{C}{q} V_{ex} \quad (3\text{-}2)$$

where C is the APD capacitor and q is electron charge and equal to $1.6021765 \times 10^{-19}$ c. In this method we try to keep V_{ex} constant. Therefore the bias voltage is estimated based on the change of breakdown voltage with change of temperature. In this mode by enabling a switch the output of quench circuit is monitored in two modes of LED-off and LED-on. Dark current rate is estimated in the case of LED-off and the sum of dark current rate and the output signal of quench circuit is measured when LED-on. With the mentioned estimations, signal-to-noise ratio is calculated.

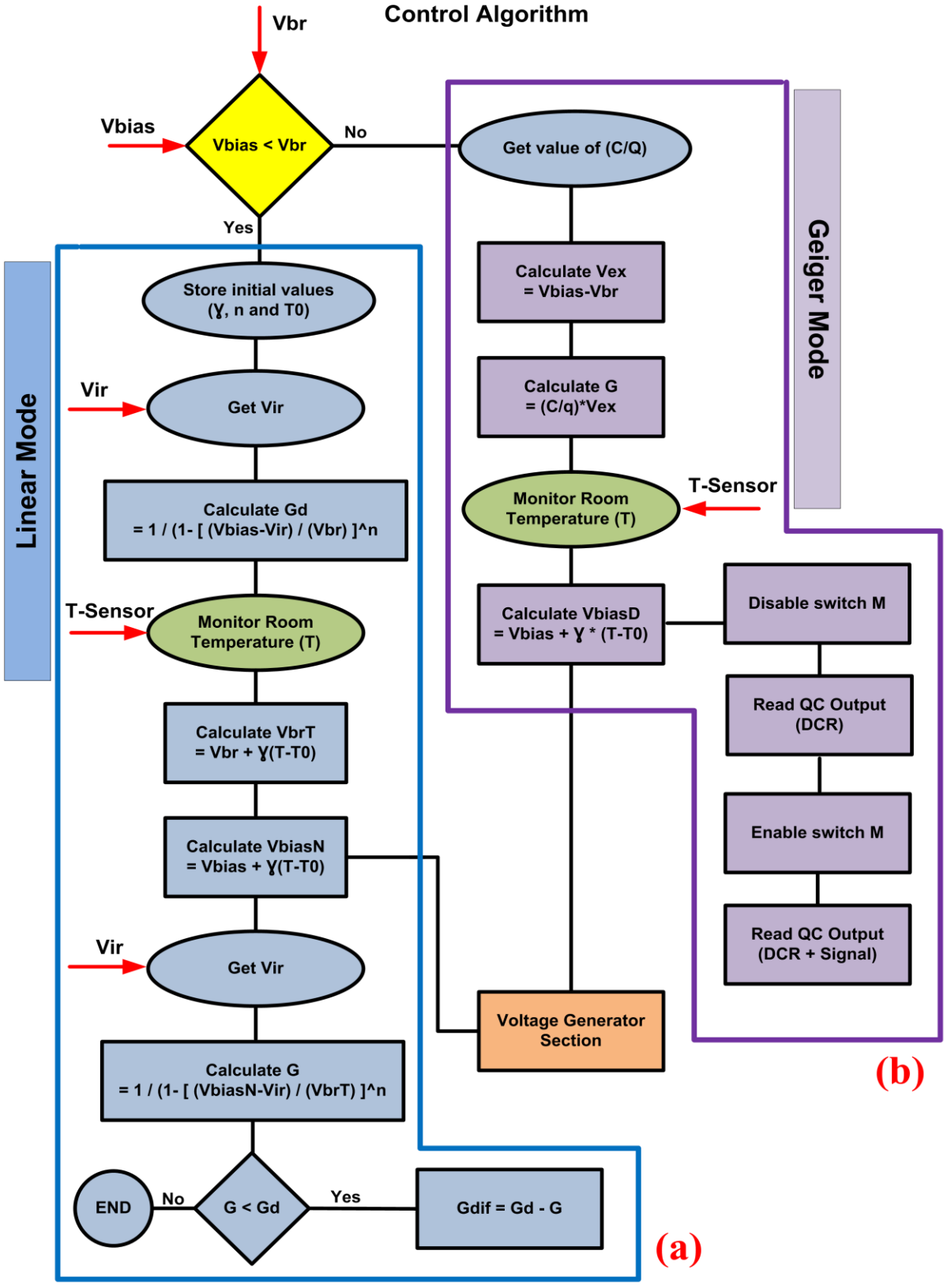

Figure 3.12: Control algorithm to compensate the thermal effect: (a) Linear-mode Algorithm, (b) Geiger-mode Algorithm

3.4 Chapter Conclusion

To verify the performance of the circuit, the transistor-level design was first captured as a schematic in Cadence's 'Schematic Editor' and all design specifications were tested. 'Virtuoso Layout Editor' from cadence was the tool used to create a compact layout design for this circuit. After the layout was completed and the Design Rule Checker (DRC) test was checked, a netlist check was performed using Layout-Versus-Schematic (LVS) to make sure that all the connections in the layout are correct and the netlist extracted from the layout matches the one extracted from the schematic. After optimization and verification of our design with aided-design (CAD) tools, the design was ready to be sent for fabrication.

The design provided a minimum dead-time of 3ns with controllable hold-off time of 1ns-2μs, and bandwidth of 1.153 GHz for the quench-reset design.

On the other side, an off-chip temperature-independent gain control system was designed and its algorithm was tested through Modelsim. In this design the effect of temperature on the gain in both linear-mode and Geiger-mode operations is controlled through changing the bias voltage of APD. After performance verification, the control system was ready to be implemented on FPGA and connected to the test APD through external connections.

CHAPTER 4 EXPERIMENTAL RESULT: QUENCH-RESET CIRCUIT AND THERMAL EFFECT CONTROL

4.1 Quench-Reset IC

The proposed quench-reset circuit was fabricated in a standard 0.18µm CMOS technology. Figure 4.1 shows the post-layout, which is designed under Cadence layout editor and simulator environment. The active area of the proposed circuit is only 50x120µm^2 with 18 pins. The supply voltage of 1.8V for analog section and 1V for digital section is chosen respectively.

The chip was fabricated by TSMC fabrication facilities through CMC Microsystems. The chip consists of different APDs and quench-reset circuits. One of the quench-reset circuits was placed separately from the designed APDs to have the option of testing quench-reset circuit independent of the APD. The overall chip is 1mm^2. Figure 4.2 presents the microphotograph of the fabricated chip, which is a zoomed-in version of the quench-reset circuit.

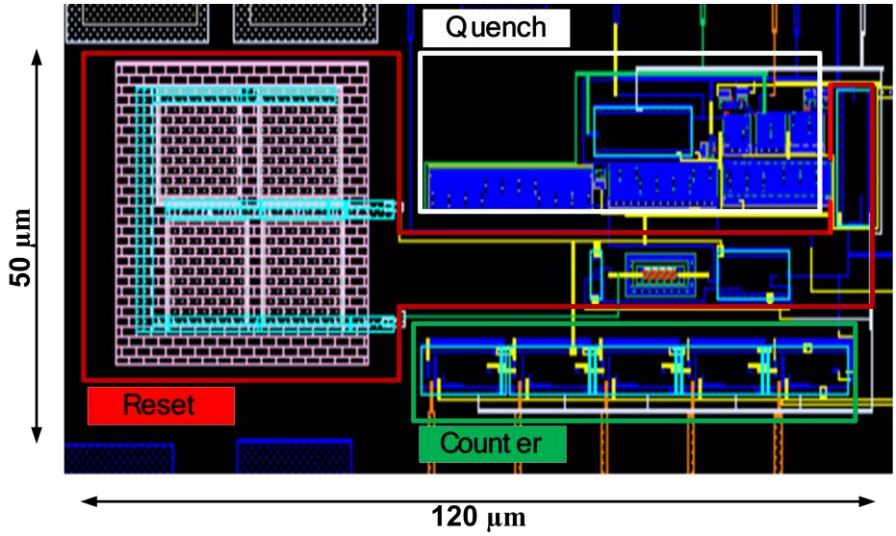

Figure 4.1: The Layout scheme of the achieved Quench-Reset Circuit

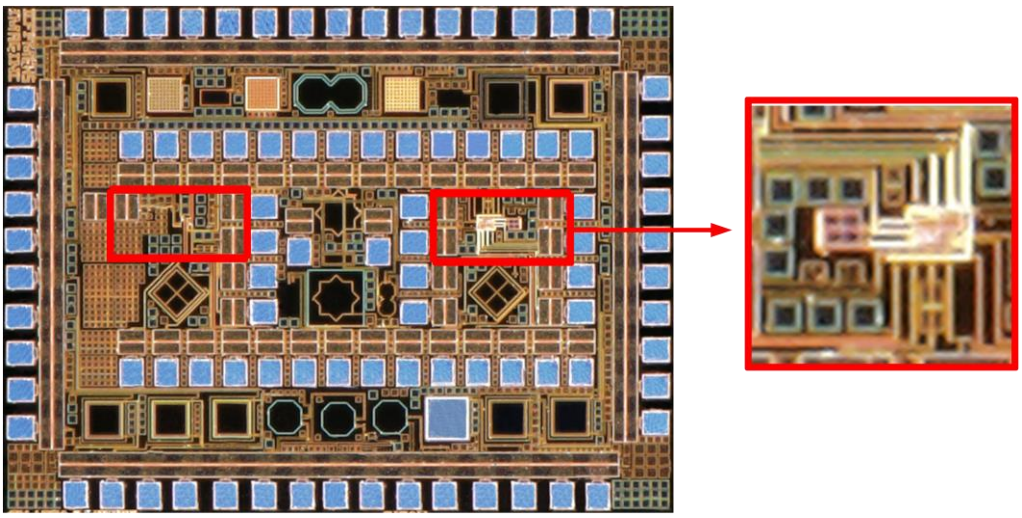

Figure 4.2: The microphotograph of the whole fabricated chip shared with a colleague from our laboratory

As explained in section 1.1 the circuit is designed to be part of the light detection section of the EEG-fNIRS brain imaging project. This whole chip includes an avalanche photodiode which is still under design improvement and test by another student within Polystim, and it is not fully functional yet. Therefore to test the functionality of the proposed quench building block, a commercially-available APD device (model S2384, Hamamatsu Company) was connected to the chip externally. As expected from the literature review, having both APD and front-end circuit integrated on the same chip will improve the quench-reset process a few hundred times faster. Therefore we are expecting to achieve quench and reset time in the range of few hundreds nanoseconds with the commercial-APD test setup.

To have the output of APD in a range similar to the output of APD proposed by Polystim, the APD model is designed based on a commercial device. Figure 4.3 depicts the APD model.

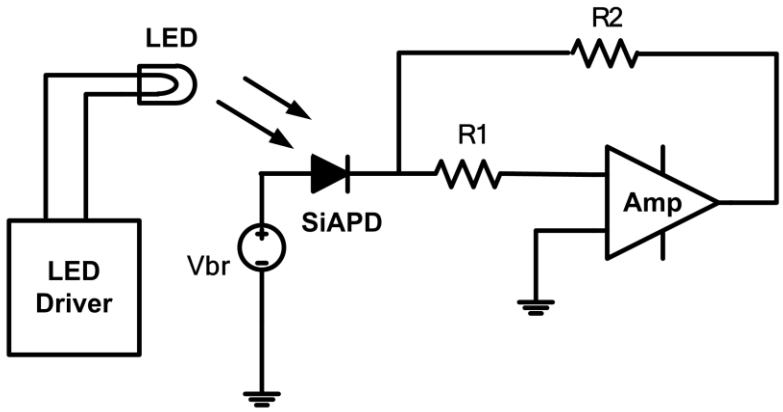

Figure 4.3: APD Model

R1 and R2 are chosen to be 12 kΩ and 10 MΩ respectively, and the amplifier is the AD8031ANZ. Hamamatsu S2384 APD active area of 3 mm, photo sensitivity at peak 0.5 A/W, cut-off frequency of 120 MHz, breakdown voltage of 150 V, terminal Capacitance of 40 pF, and gain of 60. The model is designed to behave as closely as possible to future-design photodiode by another student in Polystim.

To isolate the APD from receiving any light rather than near-infrared LED, both APD and LED are placed in a black box.

Figure 4.4 depicts the experimental setup used to characterize the proposed quench-reset circuit. The setup consists of a power supply for both digital and analog V_{dd}, and a 2-channel oscilloscope to monitor the APD cathode voltage and the digital generated pulse. Q0 – Q4 indicates the output signals of the on-chip counter, which would pass through Binary-to-seven segment decoder, and display the number of pulses in the form of 7-segment. To automatically maintain a constant voltage level for both analog and digital voltages of IC and isolate the chip from power supply small-change damage, a voltage regulator is used. The LM117 series of adjustable 3-terminal positive voltage regulators can supply in excess of 1.5A over a 1.2V to 37V output range. The output voltage of regulator is selected using two resistors. Normally R_1 is chosen to be around 220Ω or 240Ω. The formula for calculating the value of R_2 is as follows based on the required output voltage:

$$V_{Out-Regulator} = 1.25\ (1 + \frac{R_2}{R_1}) \tag{4-1}$$

Therefore the value of R_2 would be

$$R_2 = R_1(\left(\frac{V_{Out-Regulator}}{1.25}\right) - 1) \tag{4-2}$$

Setting R_2 to zero causes the output voltage to drop to 1.25V to apply to the pin connected to IC digital V_{DD}. Likewise to apply 1.8V to analog V_{DD} pin, R_2 is calculated to be 105 Ohm.

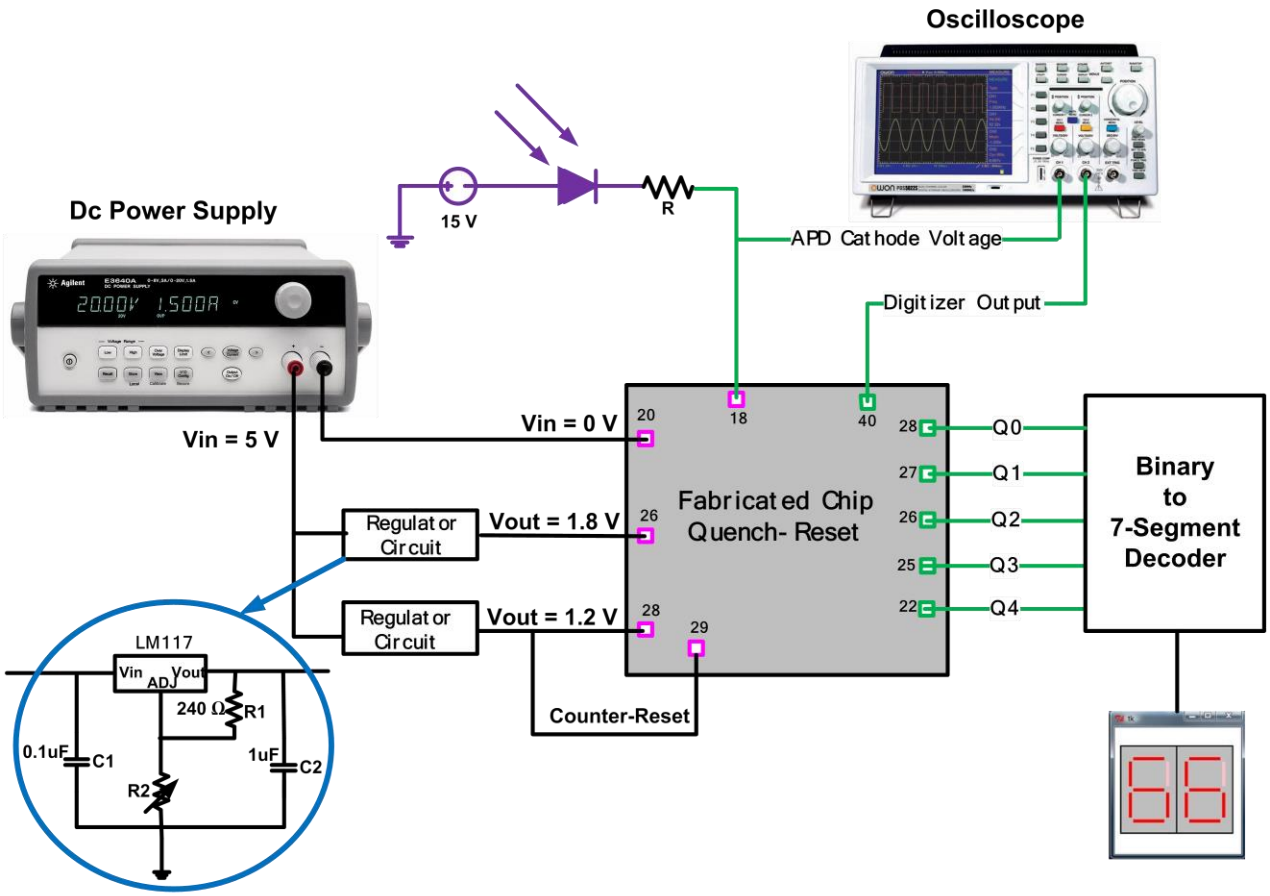

Figure 4.4: Test setup of fabricated chip

To verify the quench circuit, the chip is tested for both continuous and one-shot input signals. The input is the signal to switch on the LED. Two cases are studied in Figure 4.5. The first case is when the light is on only for short period. This input is called one shot pulse (Figure 4.5a). The

second case is when the light is on for long period and it is called continues-wave light. In post layout result one shot input can be as short as 7ns, however in measurement with non-integrated APD the minimum input is 250ns. Besides testing with non-integrated APD, the difference between measurement and post-layout results is due to the bandwidth limitation of testing devices. In Figure 4.5b the LED light is on for 2↘s and 8 pulses are detected. Thus the dead-time of each pulse is 250ns. The third signal in both Figure 4.5a and Figure 4.5b indicates the digital pulse generated with respect to each detection. Counting the number of pulses of mentioned signal in specific period indicates the speed of photon counting in Mcounts/s. On the other hand, the photon counting rate is estimated from the overall dead time, which is equal to the width of each of mentioned pulses.

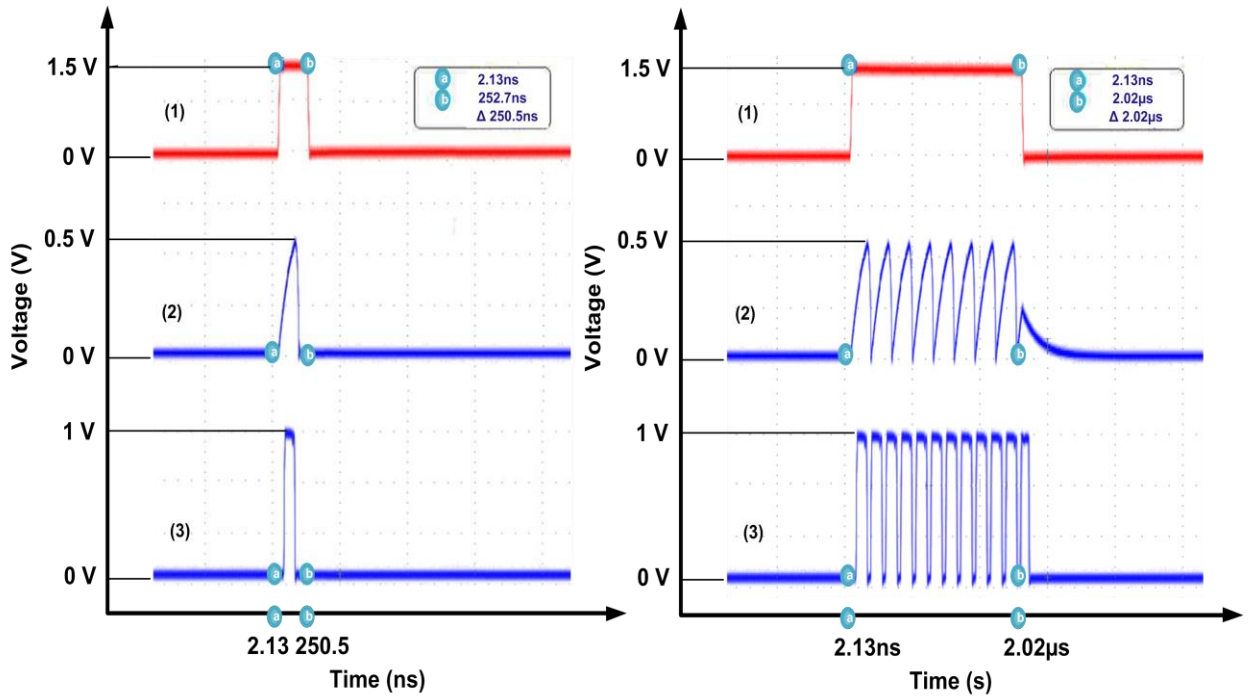

(a) (b)

Figure 4.5: Chip test result in response to: (a) one-shot light, (b) continues-wave light. In both plots: (1) LED driver voltage, (2) APD cathode voltage, (3) Output pulse to be sent to counter

To test the ability of reset block in generating different hold-off times, the monostable section of the reset block is tested with different RC. As shown in Figure 4.6, the monostable section in reset block is capable of generating reset pulse with hold-off time in the range of 4ns to 2µs. In

this figure Signal (1) in both plots indicates the output from quench circuit used for the reset block, and signal (2) indicates the output of this reset block. From the figure, we can conclude that with similar input to the reset block that depends on the hold-off time, different-width outputs can be generated. In Figure 4.6a, the generated hold-off pulse is 4ns while, Figure 4.6b shows the reset signal with hold-off time equal to 2.60µs.

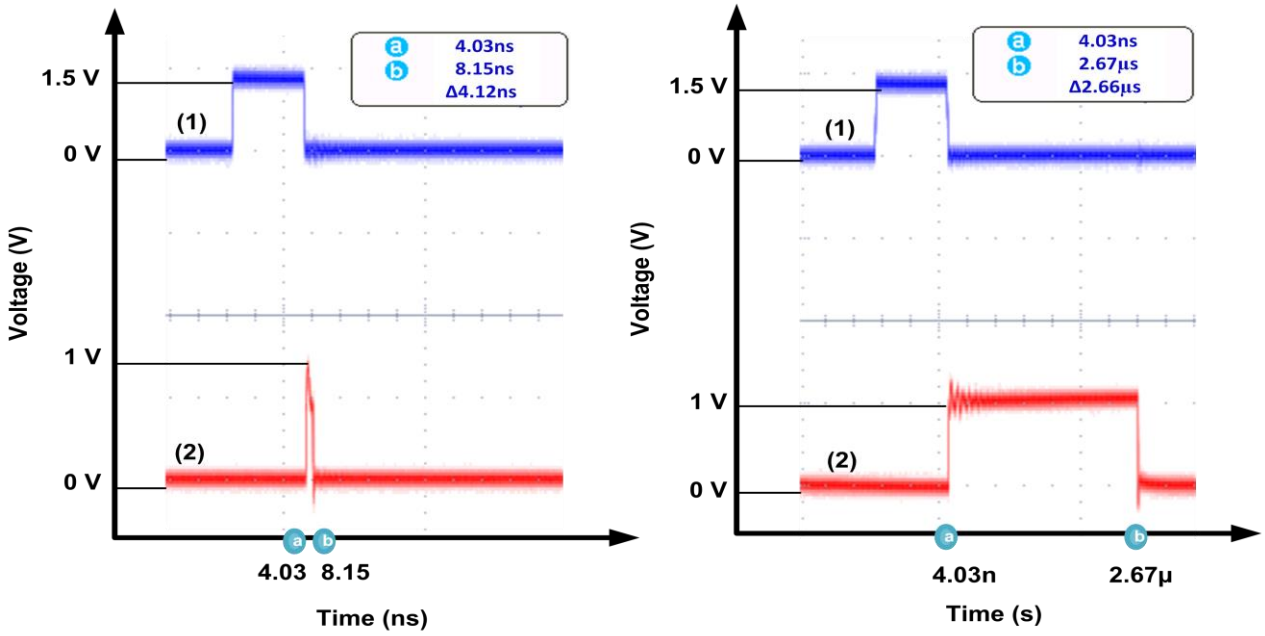

(a) (b)

Figure 4.6: Chip test result for reset circuit with: (a) hold-off time of 4ns, (b) hold-off time of 2µs. In both plots: (1) input pulse to reset block and signal, (2) output pulse of reset block

Table 4.1 summarizes the design characteristics of both circuit simulations and fabricated chip results. The power consumption, input and output impedances of IC measurement are compared with the simulation results.

Table 4.1: Design characteristics

Parameter	Simulation	Measurement
Power Consumption	2.14 mW	1.70 mW
Input Impedance	2 Ω	2.8 Ω
Output Impedance	1.58 kΩ	1.24 kΩ

4.2 Control system

The thermal effect control is designed to keep the gain of the APD in accepted range. Depending on the APD mode of operation, different algorithms may apply.

4.2.1 Controller

An inexpensive, fast, and reconfigurable control method is an FPGA programmed in a VHDL language. Igloo FPGA from Actel was chosen due to its low power consumption. The device with 100 pins adaptor and the programmer Flash Pro is shown in Figure 4.7.

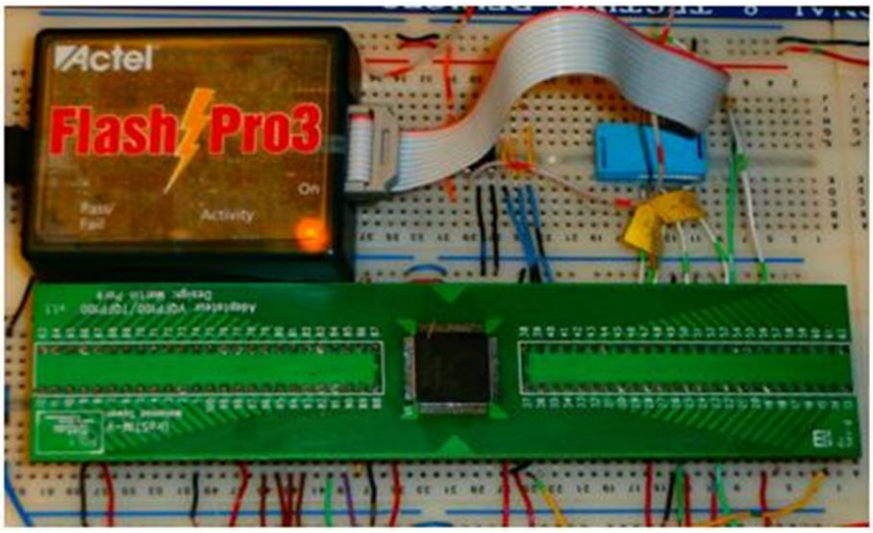

Figure 4.7: Igloo FPGA and FlashPro programmer

The code consists of the main control unit and peripheral modules. These modules are depicted in Figure 4.8. In addition, Libero is a comprehensive FPGA design and development software dedicated to Actel products. It combines Microsemi SoC Products Group (formerly Actel) tools with software such as Modelsim for simulation and Synplify for code synthesis and implementation.

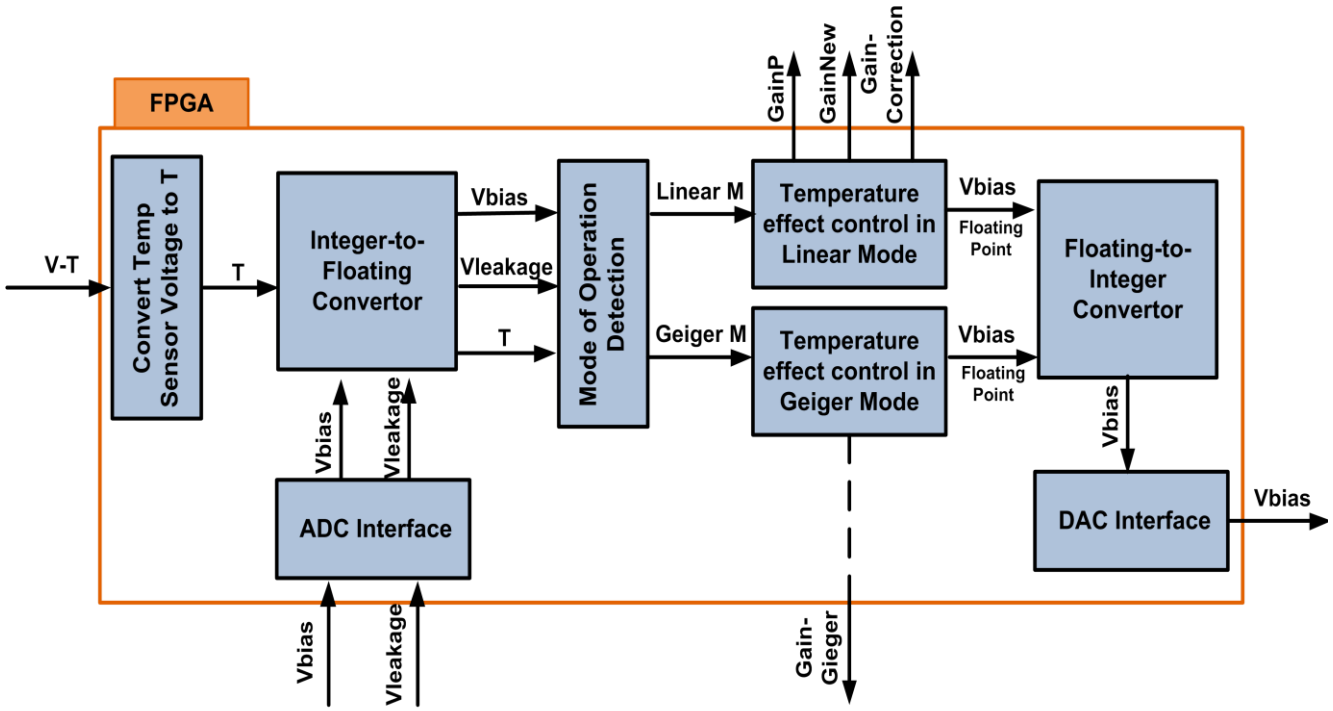

Figure 4.8: Different modules of the control unit built by a dedicated VHDL code

Inputs: These signals are:

- Breakdown voltage: which is a physical characteristic of the APD; it is a constant input in a test setup for a specific APD
- Bias voltage: which is a variable input in each loop of operation
- Leakage voltage: which is a variable input in each loop of operation; it is used in the gain calculation in linear mode. Leakage voltage is measured from the output of the TIA, which works as a current-to-voltage convertor for the leakage current of the APD
- Temperature-sensor voltage: which is linearly proportional to the temperature in centigrade degrees.

Temperature Sensor Interface: The integrated-circuit temperature sensor, LM35, generates an output voltage signal with linear scale factor of +10 mV/°C. This value is converted to temperature value by passing through the Voltage-Temperature convertor unit. In this unit the temperature is calculated by multiplying the sensor voltage by a voltage-temperature factor.
The temperature value is used in the control algorithm in both linear and Geiger modes.

ADC and DAC Interface: Analog-to-Digital (A/D) and Digital-to-Analog (D/A) convertors are used through interface modules; the mentioned code structure is device-dependent on I/O signals and control signals of A/D and D/A converters.

Integer and Floating Point Conversion Units: Due to mathematic calculations in the control algorithm, the values are required to be in floating point format. Integer-to-Floating point conversion is adopted using 8-bit integer to 64-bit floating point and pre-saved values in a memory. On the other hand, the floating-to-integer module produces integer values to communicate with the D/A converter.

Outputs: The outputs of the circuit are:

- Primary gain (GainP), improved gain (GainNew) and the correction factor (GainDiff) in linear mode of operation
- Gain in Geiger mode of operation
- Required bias voltage in both modes of operation

4.2.2 Temperature sensor

The temperature sensor, LM35, is an integrated circuit with high accuracy of 0.5˚C at room temperature and over a temperature range of −55°C to +150°C. The low-output impedance, linear output, and precise inherent calibration of the LM35 make it a suitable choice for the control circuitry. LM35 has a very low self-heating of less than 0.1°C, since it draws only 60 μA from the supply [69]. The output is the voltage signal with a linear scale factor of +10 mV/°C.

4.2.3 Test Bench

Figure 4.9 illustrates the overall test bench, which consists of an FPGA, quenching block and additional needed circuitries. To maximize the performance of the APD, its gain is monitored in each loop of operation; depending on both modes of operation (linear and Geiger modes), different actions are taken to set the optimal bias voltage. The calculated bias voltage value is sent to a D/A converter, LTC1665 from linear technology;

To set the APD bias voltage, the converted analog signal is sent to the power-set unit. As shown in Figure 4.9 the power set unit is a buffer (AD8005) which consists of two amplifiers. Besides controlling the thermal effect, depending on the mode of operation, the control signal is generated and the device switches between quench-reset circuit for Geiger mode operation and TIA for linear mode through a MAX4525 multiplexer.

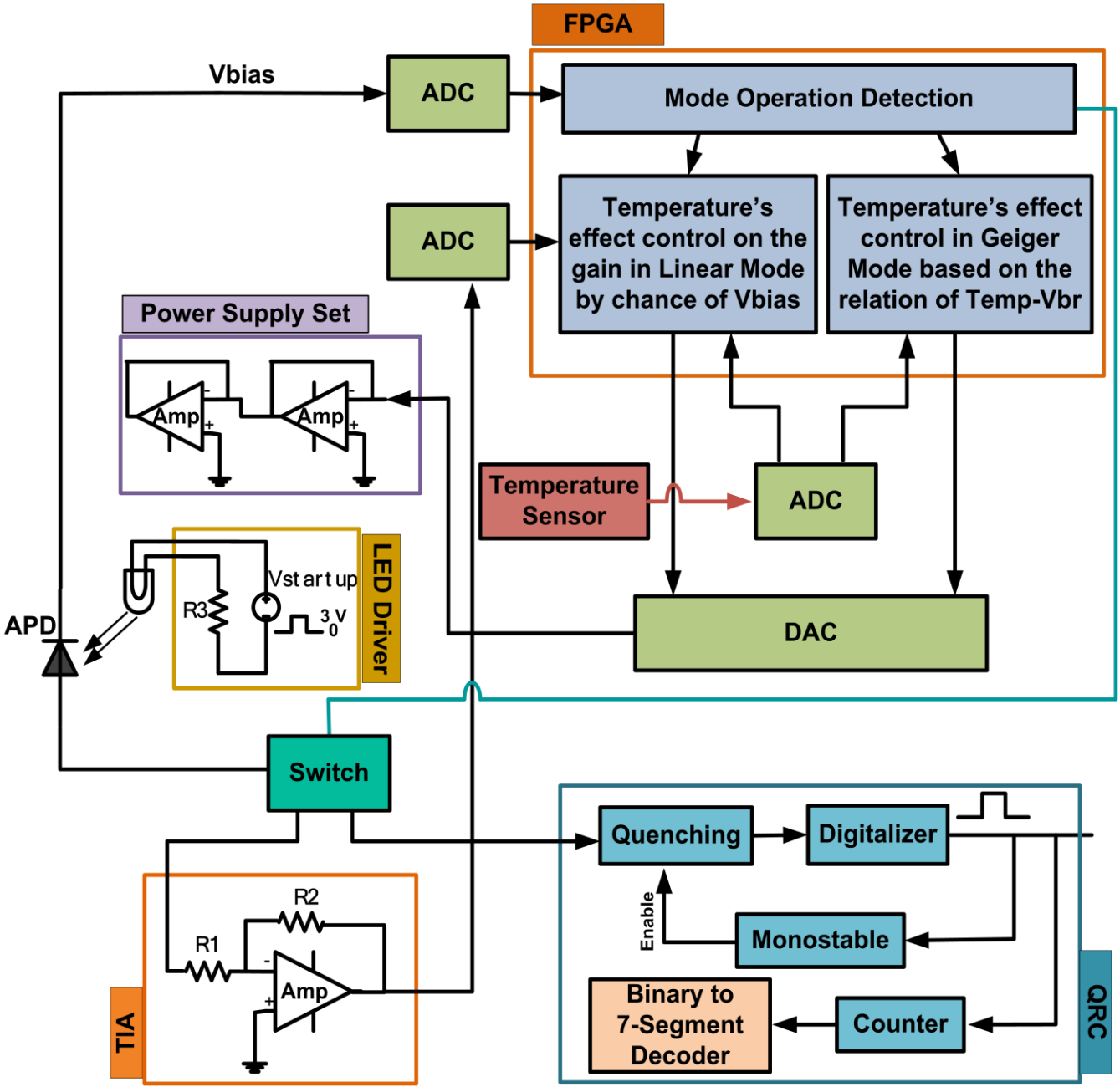

Figure 4.9: Control system test bench

4.2.4 Control System Result

4.2.4.1 Linear Mode

To test and validate the functionality of the linear-mode control loop, a test bench was created. Table 4.2 indicates the I/O list. In the table, breakdown voltage and temperature coefficient are two constant values for any specific APD. The leakage voltage is measured based on leakage current while primary bias voltage is calculated by the equation: $V_{Bias} = V_{Br} + V_{ex}$. At this point, with the help of the algorithms the primary gain is calculated and the required bias voltage is estimated to keep the gain within 10% variation. It is worth noting that the primary gain is calculated based on inputs before the temperature-independent gain loop control is applied.

Table 4.2: I/O list of thermal effect control module for linear mode APD

I/O List	Abrivation	Parameter	Value (Decimal)	Required Clock Cycles
Input (Constant)	Vbr	Breakdown Voltage	15V	-
	CoefTVbr	Temperature Coefficient	0.65	-
Input (Measured)	Vr	Bias Voltage	14.7V	-
	Vir	Leakage Voltage	0.1V	-
	T0	Primary Temperature	25°C	-
Output (Calculated)	Gd	Primary Gain	37.75	400

To verify the temperature-independent gain control, two cases are studied. In the first case, the ambient temperature is increased by 2°C, and in the second case it is decreased by 2°C. In both cases, the required bias voltage is calculated and set through power supply unit and the new gain is calculated. The goal is to have the new gain within 10% variation from the primary gain value. Table 4.3 and 4.4 present the results.

Table 4.3: 1st Study case for thermal effect control module of linear mode APD – 2°C increase in ambient temperature

I/O List	Abr.	Parameter	Value (Decimal)	Required Clock Cycle
Input	T	Secondary Temperature	27°C	-
Output	NewBias	Proposed Bias Voltage	16.1	85
	G	New Gain	41.00	427

Table 4.4: 2nd Study case for thermal effect control module of linear mode APD – 2°C decrease in ambient temperature

I/O List	Abr.	Parameter	Value (Decimal)	Required Clock Cycle
Input	T	Secondary Temperature	23°C	-
Output	NewBias	Proposed Bias Voltage	13.5	85
	G	New Gain	34.50	427

As equation (4-3) and (4-4) indicate, the new gain in both study cases has a variation of 10% in comparison to primary gain.

$$Study\ Case\ 1:\ \%\ Gain\ Variation\ = \frac{41.00 - 37.75}{37.75} = 8.6\% \tag{4-3}$$

$$Study\ Case\ 1:\ \%\ Gain\ Variation\ = \frac{37.75 - 34.50}{37.75} = 8.6\% \tag{4-4}$$

To validate the proposed algorithm, the value of gain is calculated in the absence of the proposed algorithm in the first study case (2 degree increase in temperature) with reference to equation 3-1:

$$G = \frac{1}{1 - [\frac{V_{bias} - I\ R}{V_{br} + \gamma(T - T_0)}]^n} = \frac{1}{1 - [\frac{14.8}{15 + 0.65(2)}]^2} = 5.69 \tag{4-5}$$

4.2.4.2 Geiger Mode

The control algorithm is based on the linear relation between temperature change and change in breakdown voltage, i.e. $\Delta V_{Br} = \gamma \Delta T$.

For testing this algorithm, an emulator is designed based on the specification of future-design APD with another student in Polystim.

The gain calculation is based on equation 3-2 for excess voltage of 0.5V. Due to the specification of the APD designed by our group , the junction capacitance is 1pF.

$$G = \frac{C}{q} V_{ex} = \frac{1 \times 10^{-15}}{1.602 \times 10^{-19}} (0.5) = 0.3121 \times 10^{4} = 3121 \quad (4\text{-}6)$$

As expected, a sudden change in gain value is observed in Geiger-mode APD in comparison to linear mode APD.

The proposed bias voltage follows the same changes as the breakdown voltage, therefore the excess voltage and as the result the gain would remain constant. In the Geiger mode APD, the gain variation is negligible. The input signals for Geiger mode APD are listed in Table 4.5.

Table 4.5: I/O list of thermal effect control module for Geiger mode APD

I/O List	Abr.	Parameter	Value (Decimal)
Input (Constant)	Vbr	Breakdown Voltage	15V
	CoefTVbr	Temperature Coefficient	0.65
	CdivQ	Capacitance / Elec charge	0.6242E4
Input (Measured)	Vr	Bias Voltage	15.5V
	T0	Primary Temperature	25°C

The algorithm is tested for two case studies similar to linear mode. The results are summarized in Table 4.6, and prove the functionality of Geiger-mode temperature-independent gain control.

Table 4.6: Case study for thermal effect control module of Geiger mode APD

I/O List		Value (Decimal)		Required Clock Cycle
Abr.	Parameter	1st Case Study: 2 degree increase	2nd Case Study: 2 degree decrease	
T	Temperature	27°C	23°C	-
NewBias	Proposed Bias Voltage	16.8	14.2	85
Vex	Excess Voltage	0.5	0.5	28
NewGain	Gain	3121	3121	58

4.2.5 Conclusion

The control unit is designed to compensate for the effect of temperature on gain by varying the value of bias voltage. The algorithm is based on the relation of gain, bias voltage and temperature and changing bias voltage to maintain the gain variation within 10% of primary gain.

Two separate algorithms are coded based on the operation modes of APD. The proposed bias voltage in the unit of voltage and required time in the unit of clock number are listed in separate tables. The gain variation is calculated in each of the cases.

CONCLUSION

This work is proposed to complete the design of the sensor developed by multidisciplinary research of IMAGINC group as part of the development of a real-time, noninvasive and portable NIRS/EEG signal acquisition system to communicate wirelessly with a computer and image the whole cortex while improving comfort in long duration scanning.

In this work, we designed and implemented an off-chip thermal effect control circuitry intended for an integrated APD photon counting system operating in Geiger mode. The theoretical analysis of the interface is confirmed by both simulation and experimental results.

Various publications addressing approaches to the design of quench and reset circuitry were reviewed. The importance of quench-reset circuit is highlighted for Geiger mode APD in different applications. The self-sustaining macroscopic current occurring as the result of avalanche multiplication for each photon in Geiger-mode APD is triggered. Therefore, an external force is required to reduce the electric field below breakdown onset and prepare the APD to detect any other arriving photon while protecting the APD from being damaged. Quench-reset circuitry is employed for this purpose. There are a variety of passive, active and mixed quench-reset circuits were reviewed and a high-speed active quench-reset circuit has been preferred and designed.

An electrical model is proposed to present the APD performance at photon detecting in the operation of a switch. In this model, equivalent junction capacitors and resistors of our group's desired APD are placed. The model is designed in the Cadence tool to simulate the behavior of the desired APD. The quench-reset circuitry is designed and simulated with TSMC 180nm standard CMOS process. The design is then laid out and the post-layout simulations were conducted to consider the non-idealities due to process imperfections and the significance of the parasitic effects on circuit performance. The schematics and post layout simulation results confirm a quench time of 1-3ns for the circuit which meet the requirements of high speed photon detection quench circuits in functional near infrared optical brain imaging spectroscopy. A controllable hold-off time of 4ns-2μs and a reset time of 1-4ns enhance the characteristics of the

proposed circuit among the previously cited solutions. Using the services provided by CMC Microsystems, the optimum layout was fabricated and special wire bonding was done by LASEM affiliated to Polystim laboratory. The designed circuit is proposed to be integrated with the APD designed in our research group. However, since the APD is still under test, the quench-reset circuit was tested with an available commercial APD. APD Hamamatsu S2384 was chosen and the results proved the functionality of our circuit.

As an integrated part of the project, an off-chip control scheme was also implemented with a FPGA platform to control the effect of temperature on the APD performance by monitoring the gain in both linear and Geiger modes of operation. The thermal effect is controlled through changing the bias voltage of the APD. The FPGA code is tested in Modelsim and implemented with Igloo FPGA (Actel co.). The designed system controls the gain variation in 10% of the primary value of gain for linear mode APD and with negligible gain variation for Geiger mode APD.

Future works based on our studies and experiments in this thesis can proceed in the following directions:

The photon counting system design can be improved by integrating the APD gain control loop, temperature sensor and quench-reset circuit on the same chip as the APD. Rather than avoiding extra wire connections and the capacitive effect, having integrated temperature sensor has the advantage of measuring the temperature of the APD junction rather than the ambient temperature; since the temperature which is in linear relation with the breakdown voltage is the junction temperature. It is worth noting that this does not affect the accuracy of our designed circuit because our control loop is tested with an emulator based on a commercial APD with parameters of the APD designed in our lab which is under test currently, and independent of the APD itself, but it would be a recommendation for the future integrated systems. The designed quench-reset circuit is capable of performing in 500 MHz - 1GHz range, which is a feature for high-speed APDs. In that case, to validate the design, the test instruments, including measurement instruments and power supply, should support a frequency range greater than 1 GHz. The control system can also be improved by adding a monitoring module to calculate and monitor other parameters of APD such as Quantum efficiency and signal-to-noise ratio.

In the design of the proposed system, several test pads are used to verify the performance of

different blocks. This resulted in using a larger silicon area to design the integrated chip. Since the performance of the photon counting system is approved, it is possible to reduce the number of the test points and minimize the size of the device. In the layout of the design, the pads are used as terminals but these pads do not provide electrostatic discharge protection. This was a limitation in our experimental test, and it is recommended that this protection be used for future testing.

REFERENCES

[1] P W McCormick, M G Goetting, M Dujovny, and J L Ausman, "Noninvasive cerebral optical spectroscopy for monitoring cerebral oxygen delivery and hemodynamics," *Critical Care Medicine*, pp. 89-97, 1991.

[2] D k Sokol, O N Markand, E C Daly, T G Luerssen, and M D Malkoff, "Near infrared spectroscopy (NIRS) distinguishes seizure types," *Seizure*, vol. 9, pp. 323-327, 2000.

[3] B J Steinhoof, G Herrendorf, and C Kurth, "Ictal near infrared spectroscopy in temporal lobe epilepsy: a pilot study," *Seizure*, vol. 5, pp. 97-101, 1996.

[4] M Sawan, M T Salam, S Gelinas, J Le Lan, F Lesage, and D K Nguyen, "Combined NIRS-EEG Remote Recordings for Epilepsy and Stroke Real-Time Monitoring," *Circuits and Systems (ISCAS)*, pp. 13-16, 2012.

[5] M Butti, M Caffini, A C Merzagora, A M Bianchi, G Baselli, B Onaral, P Secchi, and S Cerutti, "Non-invasive neuroimaging: Generalized Linear Models for interpreting functional Near infrared Spectroscopy signals," in *Proceeding of the 3rd international IEEE EMBS Conferance on Neural Engineering*, Kohala Coast, hawaii, 2007.

[6] S Fantini and M A Franceschini, "Chapter 7: Frequency-Domain Techniques for Tissue Spectroscopy and Imaging," in *Handbook of Optical Biomedical Diagnostics*. Bellingham, WA: SPIE Press, 2002, pp. 405-453.

[7] A Sultana, E Kamrani, and M Sawan, "CMOS silicon avalanche photodiode for NIR light detection: a survey," *Analog Integrated Circuits and Signal Processing*, vol. 70, pp. 1-13, 2012.

[8] Hamamatsu, "Chapter 02: Si photodiodes," in *Photonic Handbook*.: Hamamatsu Photonics K. K., pp. 22-66.

[9] D Dai, H Chen, J E Bowers, Y Kang, M Morse, and M J Paniccia, "Equivalent circuit model of a Ge/Si avalanche photodiode," *Group IV Photonics*, San Francisco, 2009.

[10] S M Sze and K N Kwok, *Physics of Semiconductor Devices, 3rd Edition*.: John Wiley & Sons Inc, 1969.

[11] C Canali, P Pavan, A Di Carlo, P Lugli, R Malik, M Manfredi, A Neviani, L Vendrame, E Zanoni, and G Zandler, "Experimental and Monte Carlo Analysis of Impact-Ionization in AlGaAs/GaAs HBT's," *IEEE Transactions on Electron Devices*, vol. 43, pp. 1769-1777, 1996.

[12] L E Tarof, J Yu, T Baird, R Bruce, and D G Knight, "Temperature Measurements of Separate Absorption, Grading, Charge, and Multiplication (SAGCM) InP/InGaAs Avalanche Photodiodes (APD's)," *IEEE Photonic Technology Letters*, vol. 5, pp. 1044-1046, 1993.

[13] R J McIntyre, "The distribution of gains in uniformly multiplying avalanche photodiodes: Theory," *IEEE Transactions on. Electron Devices*, vol. 19, pp. 703-713, 1973.

[14] J Cheng, "Self-Quenching Single photon Avalanceh Photodiodes for Near-Infrared Detection," University of california, 2012.

[15] F Loforce, "Low noise optical receiver using Si APD," *Proc. SPIE*, vol. 7212, Optical Components and Materials VI, no. 721210, 2009

[16] R F Pierret, *Semiconductor Device Fundamentals*: Addison-Wesley Publishing Company, 1996.

[17] F Zappa, S Tisa, A Gulinatti, A Gallivanoni, and S Cova, "Complete single-photon counting and timing module in a microscope," *Optics Letters*, vol. 30, pp.1327-1329, 2005.

[18] K Zhao, *III-V Single Photon Avalanche Detector with Built-In Negative Feedback for NIR Photon Detection*: Proquest, Umi Dissertation Publishing, 2012.

[19] D Pellion, "Modélisation, fabrication et évaluation des photodiodes à avalanche polarisées en mode Geiger pour la détection du photon unique dans les applications Astrophysiques," Ph.D. dissertation, Dept. Elect. Eng., Université Paul Sabatier-Toulouse III, 2008.

[20] B G Streetman, *Solid State Electronic Devices*. 4 edition: Prentice-Hall International, 1995.

[21] Hamamatsu, Characteristic and use of Si APD (Avalanche Photodiode), Technical Report, 2004.

[22] A Gallivanoni, I Rech, and M Ghioni, "Progress in Quenching Circuit for Single Photon Avalanceh Diodes," *IEEE Tranactions on nuclear science*, vol. 57, 3815–3826, 2010.

[23] W T Tsang, "Part D: Photodetectors," in *Semiconductors and Semimetals. Volume 22: Lightwave Communications Technology*: Academic Press, 1985.

[24] X Zheng, "Long-Wavelength, High-Speed Avalanche photodiodes and APD array", Ph.D. dissertation, Dept. Elect. Eng., University of Texas at Austin, 2004.

[25] J E Bowers and Y G Wey, "High-Speed Photodetectors," in *Handbook of Optics*. New York: McGraw-Hill, 1995, ch. 17, pp. 17.11–17.14.

[26] V H Dhulla, "Single photon counting for ultra-weak fluorescence detection: system design, characterization and application to DNA-sequencing," Ph.D. dissertation, Dept. Elect. Eng., Stony Brook University, 2007.

[27] Maxim, DS-1100, 5-Tap Economy Timing Element (Delay Line), [Online]. HYPERLINK " http://www.maxim-ic.com " http://www.maxim-ic.com

[28] K E kolb, "Characterization of silicon photodiodes with novel device architecture," Master's Thesis, Collage of Science. Chester F. Carlson Center for Imaging Science, Rochester Institude of Technology, 2011.

[29] J B Hurst, “Molecular-beam Epitaxial Growth of Low-dark-current Avalanche Photodiodes,” Ph.D. dissertation, Dept. Elect. Eng., University of Texas at Austin, 2007.

[30] T Nesheim, “Single photon detection using avalanche photodiode,” Master’s Thesis, Dept. Elect. & Telecom. Eng., Norges teknisk-naturvitenskapelige universitet, 1999.

[31] L Cheng, “Novel single photon sensors for highly sensitive fluorescence detection systems,” Ph.D. dissertation, Dept. Elect. Eng., State University of New York at Stony Brook, 2009.

[32] M A Itzler, R Ben-Michael, C F Hsu, K Slomkowski, A tosi, S Cova, F Zappa, R Ispasoiu, "Single photon avalanche diodes (SPADs) for 1.5μm photon counting applications," *Journal Modern Optics*, vol. 54, pp. 283-304, 2007.

[33] k Phang, "CMOS Optical Preamplifier Design Using Graphical Circuit Analysis," Master’s Thesis, Dept. Elect. Eng., University of Toronto, 2001.

[34] T H Lee, *The Design of CMOS Radio-Frequency Integrated Circuits*. Cambridge, U.K.: Cambridge Univ. Press, 1998.

[35] Sh Deng and A P Morrison, "Design of a Hold-off Time Control Circuit for Geiger-mode Avalanche Photodiodes," *International Journal of Microelectronics and Commputer Science* , vol. 3, pp. 53-59, 2012

[36] R J Mcintyre, "Theory of Microplasma Instability in Silicon," *Journal of Applied Physics*, vol. 32, pp. 983-995, 1961.

[37] S Cova, M Ghioni, A Lotito, I Rech, and F Zappa, "Evolution and prospects for singe-photon avalanche diodes and quenching circuits," Journal of modern optics, pp. 1267-1288, 2004

[38] SensL Company. [Online]. HYPERLINK "http://www.SensL.com" http://www.SensL.com

[39] D Rennker, "Geiger-mode avalanche photodiodes, history, properties, and problems,"

Nuclear Instruments & Methods in Physics Research Section A, vol. 567, pp. 48-56, 2006.

[40] R h Haitz, "Model for the electrical behavior of a microplasma," *Appled Physics*, vol. 35, pp. 1370–1376, 1964.

[41] P P Webb, R J Mclntyre, and J Conradi, "Properties of Avalanche Photodiodes," *RCA Review*, vol. 35, p. 234-278, 1974.

[42] J Ohta, *Smart CMOS Imge Sensors and Applications*. Boca. Raton, FL: Taylor & Francis Group, 2008.

[43] W G Lawrence, G Varadi, G Entine, E Podniesinski, and P K Wallace, "Enhanced red and near infrared detection in flow cytometry using avalanche photodiodes," *Cytometry*, vol. 73A, pp. 767-776, 2008.

[44] M M El-Desoki, "CMOS imagers for low-level light and high-speed biomedical applications," Ph.D. dissertation, Dept. Elect. Eng., McMaster University, 2010.

[45] C A Primmerman, "Detection of Biological Agents," *Lincoln Laboratory Journal* , vol. 12, pp. 3-31, 2000.

[46] S Cova, M Ghioni, A Lacaita, C Samori, and F Zappa, "Avalanche photodiodes and quenching circuits for single-photon detection," *Applied Optics*, vol. 35, pp. 1956-1963 1996.

[47] W G Oldham, R Samuelso, and P Antognet, "Triggering phenomena in avalanche diodes," *IEEE Transactions on Electron Devices*, vol. 19, pp. 1056-1060, 1972.

[48] H Dautet, P Deschamps, B Dion, A D MacGregor, D MacSween, R J McIntyre, C Trottier, and P P Webb, "Photon-counting techniques with silicon avalanche photodiodes," *Applied Optics* , vol. 32, pp. 3894-3900, 1993.

[49] W Becher, *TCSPC Handbook, 2nd ed*. Berlin: Becher & Hickl GmbH, 2006.

[50] S Felekyan, R Kuhnemuth, V Kudryavtsev, C Sandhagen, W Becker, and C A M Seidel, "Full correlation from picoseconds to seconds by time-resolved and time-correlated single photon detection," *Review of Scientific Instruments*, vol. 76, pp. 83104-83114, 2005.

[51] H Finkelstein, M J Hsu, and S Esener, "An ultrafast Geiger-mode single photon avalanche diode in 0.18-μm CMOS technology," in *Proc. SPIE 6372, Advanced Photon Counting Techniques*, 63720W, Boston, 2006.

[52] A Rochas, G Ribordy, B Furrer, P A Besse, and R S Popovic, "First passively-quenched single photon counting avalanche photodiode element integrated in a conventional CMOS process with 32ns dead time," *SPIE - The International Society for Optical Engineering*, vol. 4833, pp. 107-115, 2002.

[53] P Antognetti, S Cova, and A Longoni, "A study of the operation and performances of an avalanche diode as a single photon detector," in *Proceedings of 2nd IEEE Ispra Nuclear Electronic Symposium*, 1975.

[54] S Tisa, A Tosi, and F Zappa, "Fully-integrated CMOS single photon counter," *Optics Express*, vol. 15, pp. 2873-2887, 2007.

[55] A Rochas, P A Besse, and R S Popovic, "Actively recharged single photon counting avalanche photodiode integrated in an industrial CMOS process," *Sensors and Actuators A : Physical*, vol. 110, pp. 124-129, 2004.

[56] S Cove, "Active quenching circuit for avalanche photodiodes," U.S. Patent 4963727, October 20, 1990.

[57] M Ghioni, S Cova, F Zappa, and C Samori, "Compact active quenching circuit for fast photon counting with avalanche photodiodes," *Review of Scientific Instruments*, vol. 67, pp. 3440–3448, 1996

[58] Micro Photon Devices, "SPAD" [Online]. HYPERLINK "http://www.micro-photon-

devices.com" http://www.micro-photon-devices.com

[59] M Liu, *Infrared Single Photon Avalanche Diodes*: University of Virginia: Disseration of Doctor of Philosophy, 2008.

[60] H Finkelstein, "Shallow-Trench-Isolation Bounded Single-Photon Avalanche Diodes in Commercial Deep Submicron CMOS Technologies," Ph.D. dissertation, Dept. Elect. Eng., University of California, San Diego, 2007.

[61] C Niclass, M Sergio, and E Charbon, "A single photon avalanche diode array fabricated in deep-submicron CMOS technology," in *Design, Automation and Test in Europe, DATE 06 Proceedings*, 2006.

[62] S J Dimler, J S NG, R C Tozer, G J Rees, and J P R David, "Capacitive quenching measurement circuit for Geiger-mode avalanche photodiodes," *IEEE Select Topic in Quantum Electronic*, vol. 13, 2007.

[63] J G Rarity, T E Wall, and K D Ridley, "Single-photon counting for the 1300-1600-nm range by use of peltier-cooled and passively quenched InGaAs avalanche photodiodes," *Applied Optics Journal*, vol. 39, pp. 6746-6753, 2000.

[64] G Ribordy and D J Gautier, "Performance of InGaAs/InP avalanche photodiodes as gate-mode photon counters," *Applied Optics Journal*, vol. 37, pp. 2272-2277, 1998.

[65] T Maruyama, M Kudo, and F Narusawa, "Photodetector having a control block for maintaining a detection signal within a predetermined tolerance range," U.S Patent 657149, May 27, 2003.

[66] H L Fu, X M Zheng, and M S He, "Exact Adjustment of Single Photon Avalanche Diode Detector for the Yunnan Observatory Laser Ranging System," *Astronomical Research & Technology* , vol. 1, pp. 37-311, 2004.

[67] B Zhou, F Y Huang, D S WU, and J Liu, "A single-photon detector without cooler," in

Proceedings of SPIE 8561, Advanced Sensor Systems and Applications, Vol. 85611E, 2012.

[68] J Stewart, A Ho, R J Hofmeister, D J Douma, L G Hosking, A Weber, and J B Price, "Avalanche photodiode controller circuit for fiber optics transceiver," U.S Patent 7155133, December 26, 2006.

[69] M Maeda and M Sudo, "Bias voltage control circuitry for avalanche photodiode taking account of temperature slope of breakdown voltage of the diode, and method of adjusting the same," 6157022 , December 5, 2000.

[70] D O'Connell, A P Morrison, K G McCarthy, P Angove, and B O'Flynn, "Miniature gain and bias control circuit for avalanche photodiode," *Electronics Letters*, vol. 43, pp. 67-68, 2007.

[71] Y Li, J Wan, B Jiang, B Wang, and L Dong, "Thermo-drift Analysis and Bias Compensation of the Gain of APD," *SPIE*7055, *Infrared Systems and Photoelectronic Technology III, 70550W*, 2008.

[72] Texis Instruments, "LM35 Datasheet", Texas Instruments Incorporated, 1999. [Online]. HYPERLINK "http://datasheetreference.com/datasheets/national_LM35_datasheet.pdf" http://datasheetreference.com/datasheets/national_LM35_datasheet.pdf

[73] S Cova, A Longoni, and G Ripamonti, "Active-quenching and gating circuits for single-photon avalanche-diodes (SPADs)," *IEEE Transactions on Nuclear Science*, vol. 29, pp. 599-601, 1982.

[74] A Gallivanoni, I Rech, D Resnati, M Ghioni, and S Cova, "Monolithic active quenching and picosecond timing circuit suitable for large-area single-photon avalanche diodes," *Optics Express*, vol. 14, pp. 5021-5030, 2006.

[75] I Rech, G Luo, M Ghioni, H Yang, X Sunney Xie, and S Cova, "Photon-timming detector module for single-molecule spectroscopy with 60-ps resolution," *IEEE Journal of Selected Topics in Quantum Electronics*, vol. 10, pp. 788-795, 2004.

[76] H Dautet and J DesChamps, "Active quench circuit and reset circuit for avalanche photo diode," U.S Patent 5532474, August 2, 1999.

[77] A R Comeau, P D Deschamps, B Y Dion, and C J Trottier, "Active quench circuit for an avalanche current device," U.S Patent 5933042, July 2, 1996.